CHALMERS
UNIVERSITY OF TECHNOLOGY

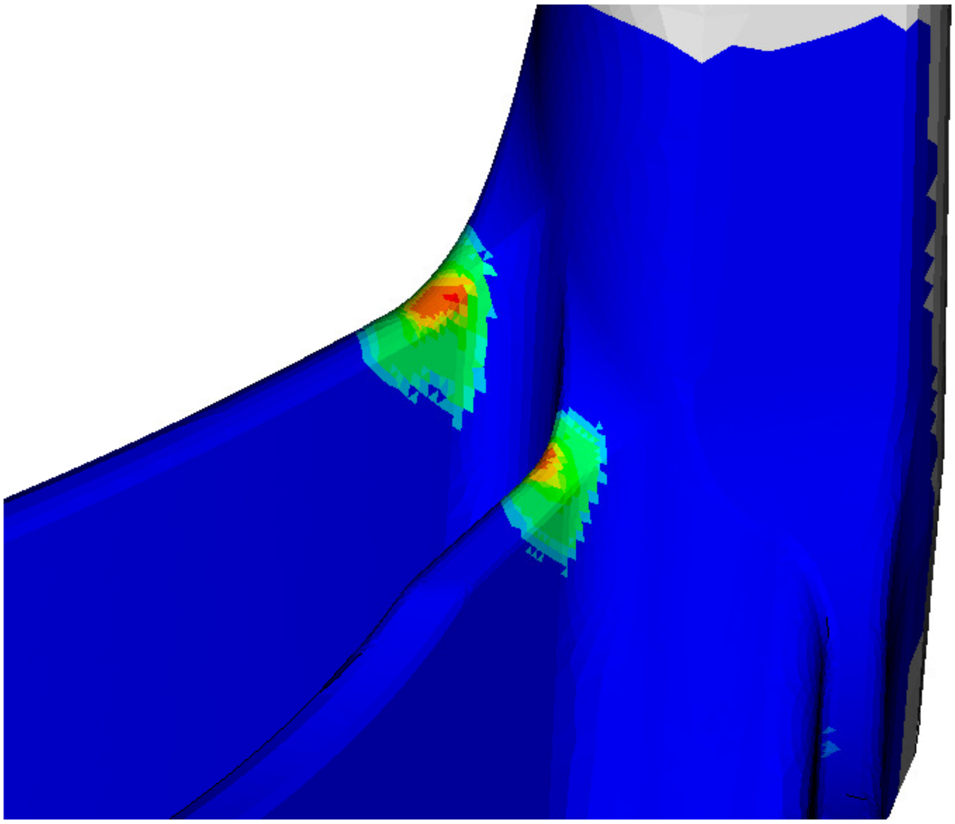

Fatigue analysis of aluminum components in powertrain mounts

Master thesis in Applied Mechanics

Caroline Bergquist

Elina Vaez Mahdavi

Department of Mechanics and Maritime Sciences
CHALMERS UNIVERSITY OF TECHNOLOGY
Gothenburg, Sweden 2019

Master's thesis 2019:08

Fatigue analysis of aluminum components in powertrain mounts

Caroline Bergquist
Elina Vaez Mahdavi

Department of Mechanics and Maritime Sciences
Division of Dynamics
Chalmers University of Technology
Gothenburg, Sweden 2019

Fatigue analysis of aluminum components in powertrain mounts
Caroline Bergquist
Elina Vaez Mahdavi

Supervisor: Daniel Högberg, Volvo Car Group
Examiner: Anders Ekberg, Department of Mechanics and Maritime Sciences

Master's Thesis 2019:08
Department of Mechanics and Maritime Sciences
Division of Dynamics
Chalmers University of Technology
SE-412 96 Gothenburg
Telephone +46 31 772 1000

Cover: Fatigue analysis plot of powertrain mounts component.

Typeset in 2019 Overleaf
Printed by Chalmers Reproservice
Gothenburg, Sweden 2019

Fatigue analysis of aluminum components in powertrain mounts
Caroline Bergquist
Elina Vaez Mahdavi
Department of Mechanics and Maritime Sciences
Chalmers University of Technology

Abstract

Components in the powertrain mounts systems withstand a large number of load cycles with varying amplitude during their operational life. Despite this, no fatigue analysis has previously been carried out of the studied components. The main aim of this study was therefore to create a method for analyzing fatigue in aluminum components in powertrain mounts. A bracket in the powertrain mounts system made of high pressure die cast aluminum EN – 46000 was in focus. The study partially aimed to account for and determine the effect of pretension on the bracket fatigue resistance. A widespread problem with fatigue analysis is the access to material fatigue parameters, and approximated material data are often employed. To investigate the consequences the influence of using various material fatigue parameters for EN – 46000 was investigated.

Based on a literature study, a strain-based approach to fatigue was selected. This allows to account for plasticity. The construction of strain – life curve combined with the establishment of a Ramberg – Osgood equation for cyclic stress – strain relationship was the basis of the fatigue analysis. Due to the mean stress that arose from the pretension, a mean stress correction following Smith – Watson – Topper was utilized. To decrease computational time, a linear elastic stress FE-analysis was carried out, Neuber correction was employed to account for local plasticity in the fatigue analyses.

Fatigue analyses of the bracket were performed with approximated material fatigue parameters using the Bäumel – Seeger method. The bracket was predicted to sustain an infinite number of load cycles. An investigation of how much larger the loads could be to sustain 4 standard operational lives was conducted. The result was 2.4 times the applied load. It was also found that small areas were affected by fatigue. Fatigue analyses were carried out with and without the pretension. A slight decrease in fatigue life was obtained without pretension due to compressive mean stresses. From a sensitivity analysis, it was concluded that employed material fatigue parameters have a significant impact on fatigue life, and that approximated material should not be used for the final fatigue analysis.

Keywords: fatigue, aluminum alloys, nCode DesignLife, pretension, strain-based, stress-based, powertrain mounts, material fatigue parameters

Acknowledgements

This Degree project was performed at the department Powertrain mounts at Volvo Car Group and the department of Mechanics and Maritime Sciences at Chalmers University of Technology in Gothenburg. The work was conducted during the spring of 2019.

Our sincere thanks to our Supervisor Daniel Högberg at Volvo Car Group who have supported and helped us throughout the whole project. He was always available to answer all the questions that we had and made time for us, which was highly appreciated. A thank you to Henrik Åkesson who always helped us with difficulties in FE-software.

We want to acknowledge Sreedhar Venkatesan and Åsa Sällström at Volvo Car Group for valuable input. We also want to take this opportunity to thank everyone at the department Powertrain mounts who made us feel welcome and made sure we enjoyed our five months there.

A special thanks to our examiner Anders Ekberg at Chalmers University of Technology for his guidance and fast replies.

Failure is not an option!

Caroline Bergquist & Elina Vaez Mahdavi
Gothenburg, June 2019

Contents

Acronyms

E – N Strain – life.

FE Finite element.

HCF High cycle fatigue.
HPDC High pressure die casting.

LCF Low cycle fatigue.
LHM Left hand mount.
LLTB Left lower tie bar.

RFC Rainflow count.
RHM Right hand mount.
RLD Road Load Data.
RLTB Right lower tie bar.
RUTB Right upper tie bar.

S – N Stress – life.
SB Subframe bracket.
SWT Smith – Watson – Topper.

UTS ultimate tensile strength.

List of Figures

List of Tables

1
Introduction

The master thesis *Fatigue analysis of aluminum components in powertrain mounts* has been conducted at Volvo Car Group at the department Powertrain Mounts. The thesis was written for a master degree in Applied Mechanics at Chalmers University of Technology.

1.1 Background

Powertrain mount systems have to isolate the body from powertrain movements, road excitation's and also limit the powertrain movements. In addition, there are noise and vibrations from the engine that the powertrain mounts have to cancel out. While these requirements have to be fulfilled, the limitations of the powertrain mounts movements have to be within the allowed packaging. The powertrain mounts also have to meet crash and safety requirements. At the same time, the components need to keep their function and efficiency during the vehicles' lifetime.

The powertrain mounts system consists of mounts, tie bars, and brackets. The mounts are called right-hand mount (RHM) and left-hand mount (LHM). The tie bars in the powertrain suspension are called right upper tie bar (RUTB), right lower tie bar (RLTB) and left lower tie bar (LLTB), see Figure 1.1 [1].

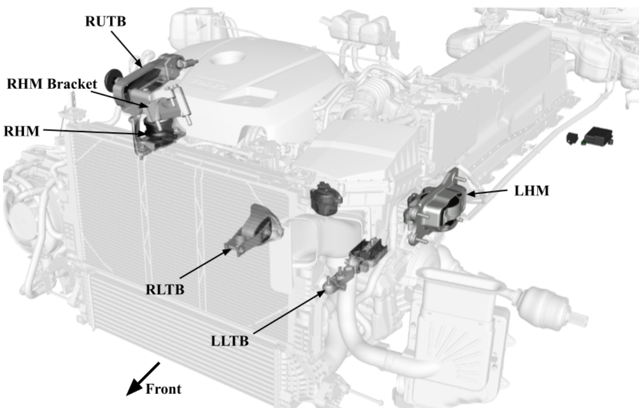

Figure 1.1: Powertrain mounts system.

The RHM is connected to a bracket made of cast aluminum. The bracket is attached to the body side, transmission, and engine with screw joints. The bracket is required for load distribution and is subjected to fatigue loads during different driving events. To evaluate the fatigue life of the bracket testing is carried out at a proving ground during extreme driving conditions. During these driving conditions, the loads on the aluminum bracket are high.

The department Powertrain mounts has so far not carried out any detailed investigation of how fatigue affects the mounts, brackets, and tie bars. Testing has so far motivated that if the brackets can handle rare extreme load events, then fatigue load driving events, at lower load levels, but with a higher number of load cycles are not critical.

The brackets are optimized for extreme driving conditions that are driving over curbs, dropping the clutch and driving in uneven conditions such as bumpy roads. Despite this, the brackets have to withstand a large number of load cycles that vary in amplitude and frequency during its operational life [2]. Therefore there was a need to evaluate how the brackets are affected by fatigue and whether it is necessary to consider fatigue when optimizing the brackets. A method for analyzing fatigue for the department Powertrain mounts had to be established. With a better understanding of how the brackets are affected by fatigue, it might be possible to improve the optimization of the brackets to decrease material use and weight.

1.2 Objectives

Fatigue analyses on rubber parts have previously been performed at the department Powertrain mounts [3]. Since no fatigue analysis had formerly been executed on the aluminum components, an investigation regarding fatigue approaches and theories was conducted.

An aluminum subframe bracket (SB) in the powertrain mounts system had previously been investigated under extreme driving events by finite element analysis (FE-analysis). To investigate if the SB could withstand a large number of load cycles during its lifetime, a method to evaluate fatigue was required. The fatigue analysis had to be able to account for the mean stress which arose the pretension in bolted joints.

Due to the possible changes in geometry and new components, direct guidelines for the method were required. Developed guidelines would make it feasible for the department Powertrain mounts to apply the fatigue analysis method on components in the future if necessary. The fatigue analyses in this study were performed in the fatigue software nCode DesignLife and in a software named Software1. Several parameters that may affect fatigue life are employed in the fatigue software. The influence of material fatigue parameters and surface roughness had to be investigated to understand the magnitude of the effect they have on predicted fatigue life.

The objectives of the current study are defined as:

- Conduct a literature study about fatigue of aluminum components.
- Gain knowledge on how fatigue analyses can be performed.
- Define a suitable method for fatigue evaluation of the SB.
- Account for mean stresses when analyzing fatigue.
- Perform a sensitivity study on parameters that affect fatigue.
- Develop guidelines for how to analyze fatigue in a suitable fatigue software while taking mean stress into consideration .

1.3 Limitations

Fatigue and FE-analyses can be time-consuming and computationally expensive because of long times series of load data and then need to employ to fine meshes in FE-analyses. To keep simulation times there are several options for. One approach employed in the current study is to carry out linear elastic analyses.

The limitations are specified below:

- The evaluated material in the SB was the aluminum alloy, EN−46000.
- Three numerical codes for fatigue evaluation were evaluated.
- No physical model of the SB was available. Therefore no validation of the fatigue results could be carried out. The method for fatigue analysis was instead applied to another component with a known fatigue life.
- Fatigue material data retrieved through physical testing were not available. Instead, the fatigue material data employed, were approximated.
- Linear elastic FE-analyses were carried out.
- Due to the complexity of the geometry no hand calculations were done to verify the FE-analyses or fatigue life results.

2
Theory

Various approaches to analyze fatigue are available for the cast aluminum SB. Properties of aluminum, manufacturing methods, surface roughness, and fatigue material data are factors that have an impact on fatigue life. Initially, an FE-analysis has to be conducted to provide input data to the fatigue analysis.

2.1 Material properties of aluminum alloys

The automotive industry often uses aluminum alloys because of their excellent properties regarding weight, strength, and resistance to corrosion [4, 5]. Depending on which alloying element that is used, different properties are obtained. The most common alloying elements are silicon, copper, zinc, magnesium, and manganese.

Aluminum – silicon are aluminum alloys that are frequently used by the automotive industry. The alloys are denoted 4xxx and are usually made by casting since the alloy has good solubility, strength and is resistant to solidification cracking. Increasing the amount of silicon makes it easier to fill the mold, especially when the component has thin walls. The cast material will also have fewer cavities when the volume of silicon increases. Having fewer cavities leads to less porosity, which improves the fatigue strength of aluminum – silicon [6, 7]. The aluminum – silicon usually has low corrosion resistance. Magnesium is beneficial to increase corrosion resistance in aluminum-silicon alloys. Aluminum – silicon with magnesium typically increases the level of corrosion resistance to almost the same level as pure aluminum [8]. Resistance to corrosion is beneficial for components in the automotive industry that are exposed to different weather conditions.

EN – 46000 (AlSi9Cu3 – (Fe)) is a commonly used aluminum – silicon alloy used in powertrain suspension, for properties of EN – 46000, see Table 2.1.

Table 2.1: Mechanical properties of EN – 46000.

Parameter	**Values**
Ultimate tensile strength (σ_u)	240 MPa
Yield strength (σ_0)	140 MPa
Young's modulus (E)	70000 MPa
Density (ρ)	2.75 kg/dm^3
Poisson's ratio (ν)	0.33

The alloy is suitable for pressure die casting and is characterized by excellent castability [9]. Another valuable property is that the aluminum alloy has limited tendency for surface and internal cavities to occur from the shrinkage during solidification.

2.2 High pressure die cast (HPDC)

Aluminum – silicon alloys, for example, EN – 46000 are commonly manufactured using HPDC [10]. More generally, powertrain components such as powertrain mounts are manufactured using HPDC. HPDC is a process where molten metal is injected under high pressure and high speed into a die. The mold is usually injected through a hydraulic ram in a containment chamber. Aluminum is (with rare exceptions) die-cast in cold chambers. When the mold enters the die and comes in contact with the thin walls in the die, the mold near the walls quickly freeze and form a skin. The skin is crucial for fatigue life, and due to its excellent quality, cast components seldom require surface finishing [5].

An intensification pressure is applied on the molten metal until the cavity is filled and a clamping force is added to prevent the die from separating. The pressure is applied to the die until the part has solidified. The intense pressure is applied to improve casting qualities [5]. The most common defects of HPDC are oxide films, porosity, and hot tears that arise during solidification [11]. The defects that occur during solidification reduce the fatigue resistance of cast aluminum alloys [12]. Fatigue failure usually initiates at the surface of the component. A larger surface area results in lower fatigue quality and the risks of defects increases [13].

2.3 Rheocasting

Rheocasting is one of many methods for semi-solid casting, and aluminum is a common material for rheocasting. The metal must contain approximately 25 to 50 % solids and 50 to 75 % liquids, to be able to cast in a semi-solid process. A semi-solid state (which is called slurry) is generated from cooling down the liquid to the accurate temperature. The slurry is injected into a die through a shot sleeve and then solidified. The slurry should have small, round grains and a well-controlled solid fraction [14]. There are various techniques for generating slurry, and that is what distinguishes different rheocasting procedures.

Unlike HPDC, there is no need to use pre-cast ingots when rheocasting. This is beneficial, since the scraps from the casting can be recycled without having to be recast into ingot [15, 16]. The defects that arise in HPDC are usually reduced with rheocasting. Regardless of this, HPDC is used more often in the industry. Gas porosity in rheocasting is decreased since the filling behavior of the die is more laminar compared to HPDC. Rheocasting gives longer die life, manufacturing time, and reduced costs compared to HPDC [11].

2.4 Finite element (FE) analyses

FEM is generally used to compute approximate solutions for partial differential equations. The method discretizes a large volume (or surface) into smaller, finite, elements. Creating an FE model can be complicated, for example, due to constraints, contacts, and irregularities. Various parameters can be employed, and simplifications are often made to limit the computational time. Since FE-analysis is an approximation method, it is crucial that the simplification results in acceptable errors and that sufficiently correct values for influencing parameters are used.

Different stress measures can be evaluated from the output from the FE-analysis. An example used in the current study is the absolute maximum principal which is defined as.

$$\sigma_a = \sigma_3 \quad \text{if} \quad |\sigma_3| > |\sigma_1| \quad \text{otherwise} \quad \sigma_a = \sigma_1 \tag{2.1}$$

where σ_1 and σ_3 are the largest and smallest principal stresses. The same approach is applicable for strains.

2.4.1 Steps in FE-analyses

In the software used in the current study, loads and boundary conditions are applied by using steps. The first step defines the boundary conditions and will be the base state for the analysis. The first step is followed by either general steps or linear perturbation steps. General analysis steps can be employed during both linear and nonlinear analysis and include the effects of the previous steps [17].

As the name states, a linear perturbation step can only be applied in linear analyses. The previous steps will not affect the next step when applying linear perturbation steps. Instead, linear perturbation steps include the conditions from the base state of the analysis [17]. Therefore linear perturbation is useful applying multiple loads but with the same boundary conditions. The output when employing linear perturbation steps separates the result from the initial step and the perturbation steps, while general step does not separate results from the different steps [18].

2.4.2 Distributing coupling constraint

A distributing coupling constraint is utilized to constrain the motion of nodes on a surface [17]. The nodes on the surface are called coupling nodes and can be observed as the yellow nodes in Figure 2.1.

A reference node is required to be able to associate the coupling nodes to a specific node when applying distributing coupling constraint. The reference node is shown in Figure 2.1 as the red node in the center. The coupling nodes may be constrained in translation and rotation with respect to the reference node. The constraint distributes loads such that the resultant of the forces and moments at the coupling nodes are equivalent to the forces and moments in the reference node [19]. In Figure 2.1, an example of distributing coupling is shown, and the connections between the reference node and coupling nodes can be seen.

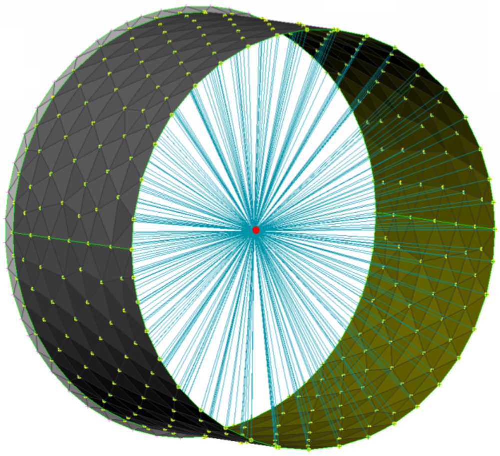

Figure 2.1: Distributing coupling between coupling noes (yellow) and reference node (red).

2.5 Fatigue analyses

Failure does not only occur when stresses exceed the strength of the material during high static loads. Repeated cyclic loading that causes fatigue failures is a common problem for metal structures and can occur below the strength of the material. In general, fatigue failures start with a small crack that grows during cyclic loading until final failure occurs [24].
Fatigue is commonly divided into low cycle fatigue (LCF) and high cycle fatigue (HCF). The region for LCF and HCF is generally separated around 10.000 cycles, although other factors affects the definition. In LCF, a significant amount of plastic deformation is generally present and the main cause of the fatigue damage. Generally, a strain-based approach to fatigue is utilized to analyze LCF. For HCF, the strains that occur are primarily elastic. Stress-based approaches to fatigue analyses are commonly utilized in HCF, although strain-based approaches to fatigue can also be employed [24].

2.5.1 Cumulative damage

The Palmgren – Miner rule is a linear damage accumulation hypothesis for loading with varying amplitudes. Fatigue damage, D is computed as

$$D = \frac{N_1}{N_{f1}} + \frac{N_2}{N_{f2}} + \frac{N_3}{N_{f3}} + ... = \sum_{i=1}^{I} \frac{N_i}{N_{fi}} \tag{2.2}$$

In equation (2.2), $\mathrm{N_i}$ is the number of load cycles, and $\mathrm{N_{fi}}$ is the number of cycles to failure at a certain load amplitude. The result of the equation (2.2) is a measurement of how much the component has been damaged. If the sum of the fractions reaches one, fatigue failure is predicted to occur. The inverse of equation (2.2) results in fatigue life in terms of the number of repeats of the load history before failure, see equation (2.3) [24].

$$N_r = \frac{1}{D} = (\sum_{i=1}^{I} \frac{N_i}{N_{fi}})^{-1} \tag{2.3}$$

2.5.2 Strain-based fatigue analysis

Detailed analysis of fatigue due to local yielding, a strain-based approach is suitable. Such a strain-based approach accounts for plastic deformation that may occur in regions of a component [24]. The strain-based approach requires a cyclic stress-strain relationship that relates stress and strain amplitude. In the current study the Ramberg – Osgood relationship is used.

$$\epsilon_a = \frac{\sigma_a}{E} + (\frac{\sigma_a}{K'})^{1/n'} \tag{2.4}$$

ϵ_a is the strain amplitude, and σ_a the stress amplitude. K′ cyclic strength hardening coefficient, and n′ cyclic strength exponent. Strains are often computed in a linear (elastic) analysis to decrease computational demands and needs for material data. Stresses beyond the yielding point, σ_0, might occur at a local stress concentration, such as in notches (see Figure 2.2) and need to be accounted for.

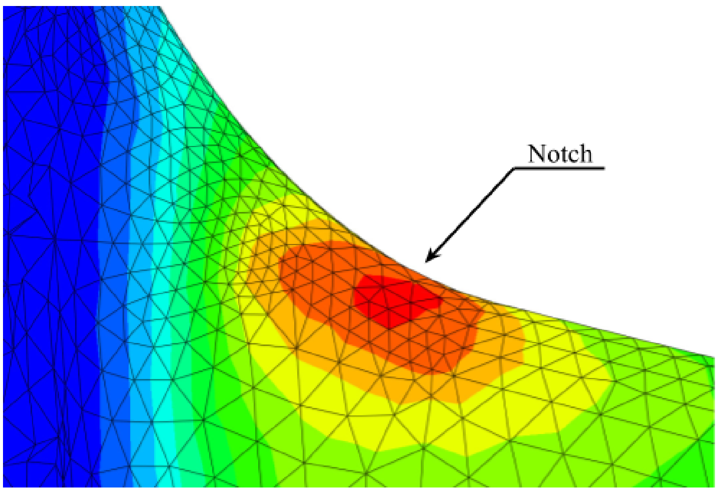

Figure 2.2: Example of a notch.

A plasticity correction estimates the amount of plasticity from an elastic analysis. One such estimate is Neuber's rule [24]. If plasticity occurs and the material is assumed to be elastic, perfectly plastic the strain can be estimated as

$$\epsilon = \frac{(K_t S)^2}{\sigma_0 E} \qquad (\epsilon \geq \sigma_0/E) \tag{2.5}$$

where S is the normal stress and the stress concentration factor K_t is defined as

$$K_t = \frac{local\ stress\ at\ notch}{nominal\ stress} \tag{2.6}$$

Large areas should not be affected by plastic strain when applying Neuber's rule in linear analysis; the stresses used in equation (2.6) have to be elastic stresses. If larger areas are affected by plastic strain, an elasto – plastic FE-analysis should be performed instead [24].

Equation (2.7) is called the Basquin – Coffin – Manson and is used for analyzing low-cycle fatigue. Basquin – Coffin – Manson describes the relationship between strain amplitude, ϵ_a, and the number of cycles, N_f, the material can sustain before failure. The material is characterized by, the fatigue strength coefficient σ'_f, the fatigue ductility coefficient ϵ'_f,the fatigue strength exponent, b and the fatigue ductility exponent c. Further the constant E is Young's modulus.

$$\epsilon_a = \frac{\sigma'_f}{E}(2N_f)^b + \epsilon'_f(2N_f)^c \tag{2.7}$$

The first term in equation (2.7) accounts for elastic strain and the second term for plastic strain. The fatigue life for the elastic strains and plastic strains are added to form the strain – life (E – N) curve, see Figure 2.3.

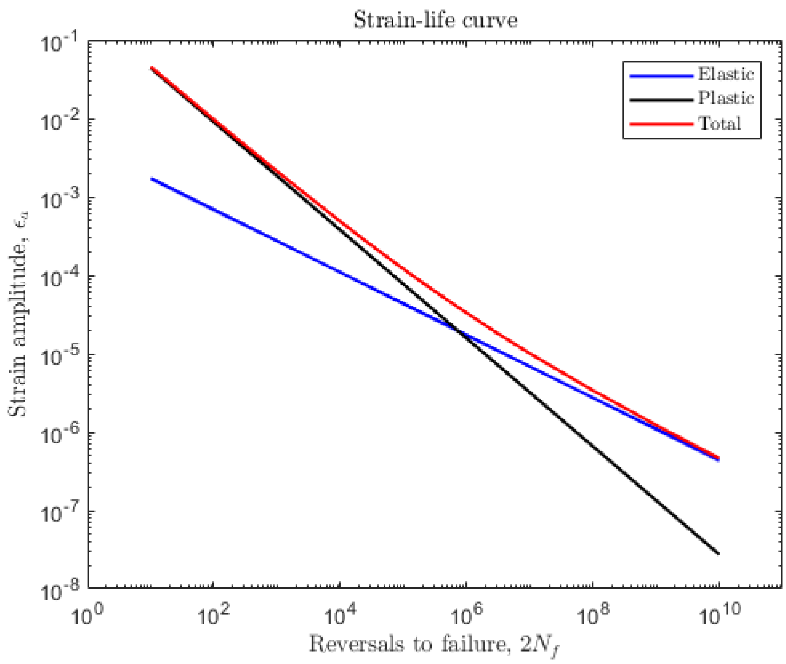

Figure 2.3: Strain – life curve.

If a mean stress is present, it is not sufficient to analyze fatigue with equation (2.7). Mean stress corrections should be utilized. The Smith – Watson – Topper (SWT) criterion is a suitable mean stress correction for aluminum alloys [24]. SWT describes the relationship between strain amplitude and fatigue life and is defined as

$$\sigma_{max}\epsilon_a = \frac{(\sigma'_f)^2}{E}(2N_f)^{2b} + \epsilon'_f\sigma'_f(2N_f)^{b+c} \tag{2.8}$$

The maximum stress, σ_{max} can be expressed as

$$\sigma_{max} = \sigma_m + \sigma_a \tag{2.9}$$

where σ_{m} is the mean stress σ_{a} is the stress amplitude.

A compressive mean stress results in a lower strain amplitude and therefore a longer fatigue life, while tensile mean stress accomplishes the opposite.

2.5.3 Stress-based fatigue analysis

Stress-based approaches are commonly employed in HCF where the deformations are primarily elastic, and plasticity does not need to be accounted for in the fatigue analysis. Fatigue life is computed with the help of a Stress – life (S – N) relationship[24]. A basic S – N curve describes the relationship between stress amplitude and the life when the mean stress is zero. This can also be expressed as if the ratio R is equal to −1. The stress ratio R is defined as

$$R = \frac{\sigma_{min}}{\sigma_{max}} \tag{2.10}$$

where R = −1 implies that there is no mean stress. If a mean stress is present (R ≠ −1) mean stress correction has to be employed. A commonly used mean stress correction for the stress-based approach is the Goodman relationship defined as

$$\frac{\sigma_a}{\sigma_{ar}} + \frac{\sigma_m}{\sigma_u} = 1 \tag{2.11}$$

where σ_{ar} is equivalent stress amplitude for R = −1. For a detailed description of the stress-based approach to fatigue, see reference [24].

2.5.4 Fatigue material data for strain-based fatigue analysis

Four material fatigue parameters are required in the Basquin – Coffin – Manson equation to be able to carry out a strain-based fatigue analysis. Test specimens are subjected to cyclic uniaxial loading to obtain the E – N curve. From the E – N curve, it is possible to determine the four material fatigue parameters; σ'_{f}, ϵ'_{f}, b and c. These tests are expensive to perform and cannot be implemented in the early design phase when various materials are under investigation [25]. Therefore it is convenient to estimate the parameters from monotonic testing. Two other parameters that are required for strain-based fatigue analysis are K′ and n′ from Ramberg – Osgood relationship.

Bäumel – Seeger and Medians method are two methods for estimating fatigue parameters from monotonic tensile test data [25, 26]. Both methods estimate σ'_f from the ultimate tensile strength (UTS), and the remaining fatigue parameters are presumed constant for all aluminum alloys. The fatigue parameters for aluminum alloys are shown in Table 2.2.

Table 2.2: Bäumel – Seeger method and Medians method for aluminum alloys.

Parameter	**Bäumel – Seeger**	**Medians method**
σ'_f	$1.67{\cdot}\sigma_u$	$1.90{\cdot}\sigma_u$
ϵ'_f	0.35	0.28
b	-0.095	-0.11
c	-0.69	-0.66
n'	0.11	-
K'	$1.61{\cdot}\sigma_u$	-

Bäumel – Seeger method has values for n′ and K′, where K′ is estimated using the UTS. For the Medians method, no constants for n′ and K′ are available; however, approximated values can be obtained from equation (2.12). By using equation (2.12), it is assumed that Ramberg – Osgood's elastic and plastic strain ranges correlate perfectly with Basquin – Coffin – Manson's strain ranges. Under that assumption, the relationship for n′ and K′ is described as in equation (2.12) [27].

$$K' = \frac{\sigma'_f}{(\epsilon'_f)^{b/c}}, \qquad n' = \frac{b}{c} \tag{2.12}$$

Neither Bäumel – Seeger or Medians method is recommended for final fatigue evaluation. The methods should only be used temporarily and as an indication of whether the component will sustain the desired number of repeats. To obtain reliable material fatigue parameters, measurements should be performed independently for σ'_f, ϵ'_f, b, c, n′ and K′ to obtain correct values [27].

2.5.5 Surface roughness

Surface roughness affect fatigue life in HCF regions more than in LCF regions. Since the elastic strains is dominating in HCF [26], the slope of the elastic part of the E – N curve is modified.

Two types of surface roughness parameters are the Arithmetic Mean Roughness parameter (Ra), and the Average Depth of Roughness parameter (Rz). The value of Ra is computed as

$$Ra = \frac{1}{n}\sum_{i=1}^{n}|y_i| \tag{2.13}$$

where n is the total number of points evaluated, and y_i is the height of the surface profile from the centerline axis in the i-th position. Rz is derived as

$$Rz = \frac{1}{5}\sum_{i=1}^{5} Y_i \tag{2.14}$$

where Y_i is the arithmetic mean of the distance between global maximum and minimum of five measurements [28], see Figure 2.4.

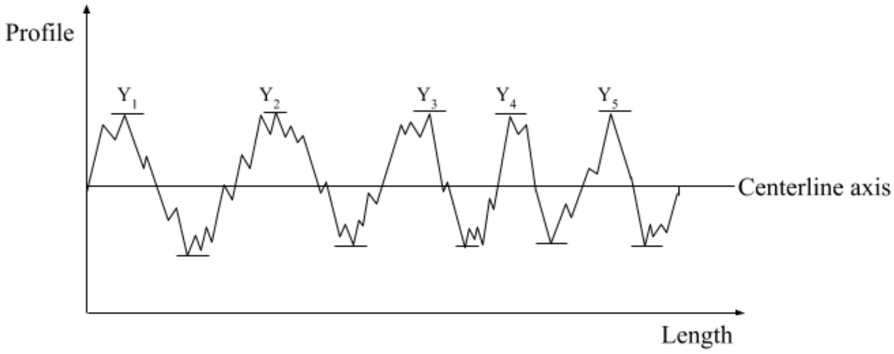

Figure 2.4: Surface profile with a centerline axis.

In nCode DesignLife [29] surface roughness is includes in a surface factor K_{sur} that is applied to the fatigue strength of the material.

$$K_{sur} = K_{Treatment} \times K_{User} \times K_{Roughness} \tag{2.15}$$

$K_{Treatment}$ is a factor that takes the surface treatment into account, K_{User} is a factor used for an unspecified reason, and $K_{Roughness}$ is a factor that takes the surface roughness into account. $K_{Roughness}$ is defined in three ways. The first option is to use the predefined surface roughness conditions that are specified in Table 2.3 [26]. Smoother surfaces that result from more precise machining, in general, improves resistance against fatigue, although some machining procedures are harmful, as they introduce tensile residual stresses [24].

Table 2.3: Surface roughness conditions.

Conditions	**Rz** [μm]
Polished	0
Ground	12.5
Machined	100
Poor machined	200
As rolled	200
As cast	200

The second option for specifying $K_{Roughness}$ is to enter a user-defined value of R_z. nCode DesignLife calculates $K_{Roughness}$ as in equation (2.16).

$$K_{Roughness} = \begin{cases} 1 \quad \text{if} \quad R_z \leq 1\mu m \\ 1 - a_R \cdot \log(R_z) \cdot log(2\sigma_u/\sigma_{u,N,min}) \quad \text{if} \quad R_z > 1\mu m \end{cases} \tag{2.16}$$

σ_u has to be stated in MPa and a_R and $\sigma_{u,N,min}$ are constants. For cast aluminum alloys $a_R = 0.20$ and $\sigma_{u,N,min} = 133$ MPa. The third option is described in nCode DesignLife theory guide [26].

3
Current analyses

An internal investigation was carried out to gain knowledge about current use of fatigue evaluation and methods for how to analyze fatigue. Among available fatigue software, nCode DesignLife and FEMFAT [30] were in use by the contacted departments. The departments utilize both strain-based fatigue analyses and stress-based fatigue analyses.

3.1 nCode DesignLife

Before fatigue analysis can be executed, an FE-analysis is required. Pretension from bolted joints results in mean stress and is applied as a general step in the FE-analysis to be able to account for the pretension in the fatigue analysis. External loads are applied and can be prescribed either as general steps or linear perturbation steps, see Section 2.4.1. After the loads are applied, an elastic FE-analysis is executed to obtain stresses and strains.

Depending on whether general steps or perturbation steps are used for applying loads, the pretension is handled differently in the fatigue software. If general steps are used, the pretension must be removed from the cyclic loading and then added as a constant. If employing perturbation steps, the pretension is added as a static load directly.

nCode DesignLife, as well as other fatigue software, gives the possibility to do both stress-, and strain-based fatigue analysis. Both stress- and strain-based fatigue analyses are used widely within different departments. Regardless if a strain-based or a stress-based fatigue approach is used, the fatigue loads are handled in the same way; a duty cycle is created containing fatigue load history.

Since the FE-analysis is linearly elastic, Neuber's rule is applied as a plasticity correction for the strain-based approach to fatigue. Neuber's rule should not be used if large plastic areas arise. In such cases, the component has to be redesigned.

When accounting for mean stress while using a strain-based approach, the SWT relationship is applied. The most common mean stress correction for a stress-based approach is Goodman relationship [26]. To employ the stresses and strains from the FE-analysis in the fatigue analysis, absolute maximum principal stress (equation

(2.1)) is used for both strain- and stress-based approach [26].

3.2 FEMFAT

Departments also use FEMFAT; however, it is employed mainly for evaluating the safety against fatigue initiation through obtaining a safety factor. It is more desirable in this study to investigate how much damage the component is exposed to. Therefore, no further investigation of FEMFAT was carried out.

3.3 Static analysis of extreme loads

At the department of Powertrain mounts, static analyses were conducted on the SB in question. The purpose of the analyses was to investigate whether or not the SB would deform or fail during extreme driving conditions. Maximum loads were applied on the SB to represent the extreme driving conditions and were added in x-, y-, and z-directions. The material for the analysis was the aluminum alloy $EN-46000$ with a yield limit of 140 MPa and a UTS of 240 MPa .

Although the loads were high, the stresses were not near the yield limit for the aluminum alloy $EN-46000$. That concludes that the SB will not break due to plastic collapse.

4

Numerical analysis

As mentioned in Section 1.2, a bracket made of HPDC aluminum, EN-46000, was analyzed during this study. The bracket is attached to the subframe, and above the bracket, there are two bushings connected. The combination of these parts holds the engine in place. The bracket had to be modeled in an FE-software to obtain stress results that could later be employed in the fatigue analysis. The stresses are presented in terms of normalized stresses ($\sigma_{\text{norm}} = \sigma/||\sigma||$) where $||\sigma||$ is a normalization coefficient.

4.1 Pre-processing

The bracket was meshed in the pre-processor ANSA Version 19.1.0 [32] with tetrahedral, 1st order elements called C3D4, see Figure 4.1. The bracket, together with neighboring parts, was analyzed with linear elastic analysis in the solver Abaqus/-Standard Version 2017.

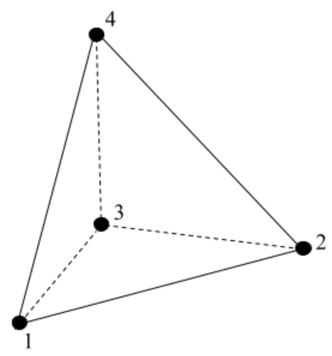

Figure 4.1: C3D4 element.

4.1.1 Boundary conditions and constraints

The aluminum bracket was attached to the subframe. Sections of the subframe were removed to minimize computation times of the analysis; the remaining segments of the subframe were kept to retain the stiffness of the bracket. All degrees of freedom on the edges of the remaining subframe were set to zero..

Distributing coupling was applied in the bushings attached to the bracket, see Section 2.4.2. The reference nodes were chosen as the center node in each bushing. In all contact areas, the contact between surfaces were defined using contact pairs.

4.1.2 Modelling of bolted joints

The model that was evaluated for fatigue had ten bolted joints. The applied pretension in the bolts varied depending on the size of the bolts. The pretension was modeled by performing a zone cut in the bolts above the threaded part. A surface was added in the zone cut, and the pretension was applied in the direction of the bolts.

The stresses that arose from the pretension had to be kept in the model to be accounted for when performing the fatigue analysis. Two static steps were created to apply and fix the pretension. The first step contained the applied pretension and boundary conditions. In the second step, the displacement which occurred from the pretension had to be fixed. The pretension was fixed by setting one degree of freedom of one node that was in contact with the bolted joint to zero. The same procedure was repeated for all bolts and the second step would act as a base state in further analyses.

4.1.3 Applied loads

External loads were added in the FE-analysis as linear perturbation steps, see Section 2.4.1. Linear perturbation steps were beneficial for the fatigue analysis since it distinguished the results from the external loads from those due to the pretension.

Unit loads were applied in x-, y- and z-direction in the reference node of both left and right bushing. The loads were distributed into the bracket through the bushings via the distributing coupling constraint. Distributing coupling constraint is explained in Section 2.4.2. The left and right bushing are identical; a schematic image of the bushing connected to the bracket with applied loads is shown in Figure 4.2.

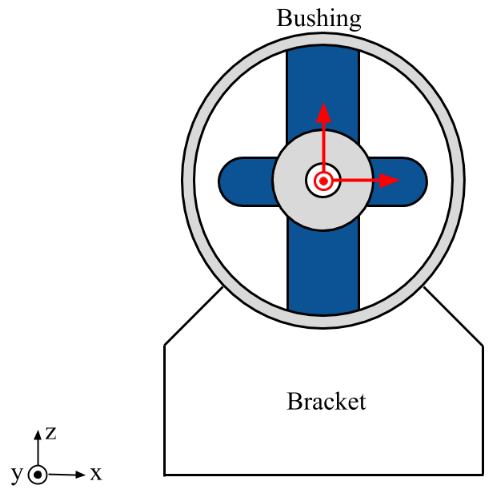

Figure 4.2: Applied loads in a schematic image of bushing and bracket.

4.1.4 Mesh convergence study

It was necessary to perform a mesh convergence study to ensure a sufficient resolution of local stresses and strains, and therefore, sufficiently accurate fatigue predictions. The computational time of the fatigue analyses was dependent on the mesh. Using an as coarse mesh as possible, but having a sufficiently fine resolution would decrease the computational time. The areas with high stress concentrations in the bracket were known from the extreme static analyses, see Section 3.3. These areas were re-meshed into a finer mesh for each analysis. The number of elements for the bracket is shown in Table 4.1.

Table 4.1: Number of elements for the meshes.

Mesh	Number of elements
1	189446
2	195446
3	199410
4	210517
5	245560
6	275310
7	305855
8	412480
9	447586
10	514152

For the mesh convergence analysis featuring pretension, the highest stress concentration was not selected, since it appeared in the contact areas of the bolted joints. The stresses from the pretension were measured in the area of circle 1, see Figure 4.3, and the same area was employed for the external load added in the x-direction in the right bushing. The area of circle 2, see Figure 4.3 has been utilized for the y- and z-direction in the right bushing. The corresponding areas have been employed for the mesh convergence analysis for loads added in the left bushing.

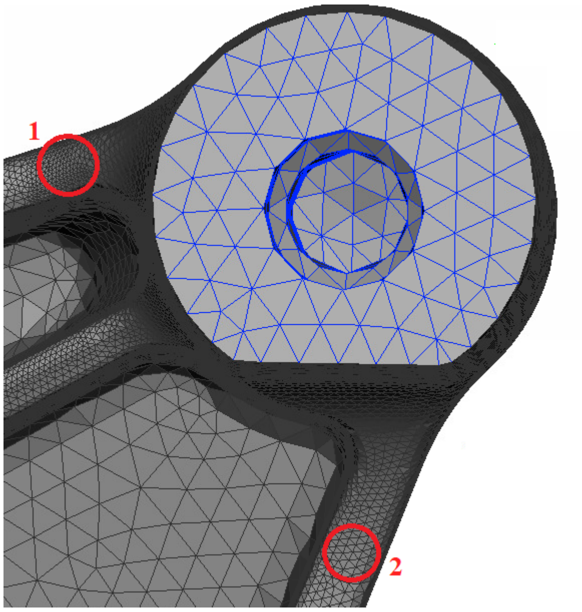

Figure 4.3: Areas for investigation of mesh dependency convergence.

4.2 Post-processing

The model was post-processed in Abaqus/Viewer 2017 [33] by analyzing the obtained stresses from the external loads and the pretension. Due to the use of linear perturbation steps, it was feasible to study stress results from each external load at a time. The convergence studies were carried out in MATLAB 2015 [34].

4.2.1 Mesh convergence study

The results from the stress convergence study are presented in Figure 4.4 and Appendix A. Figure 4.4 shows the stresses for all ten meshes, obtained from adding external loads to the right bushing in the x-direction. It can be stated that the stress magnitude has converged at Mesh 6 with a slight deviation for Mesh 10.

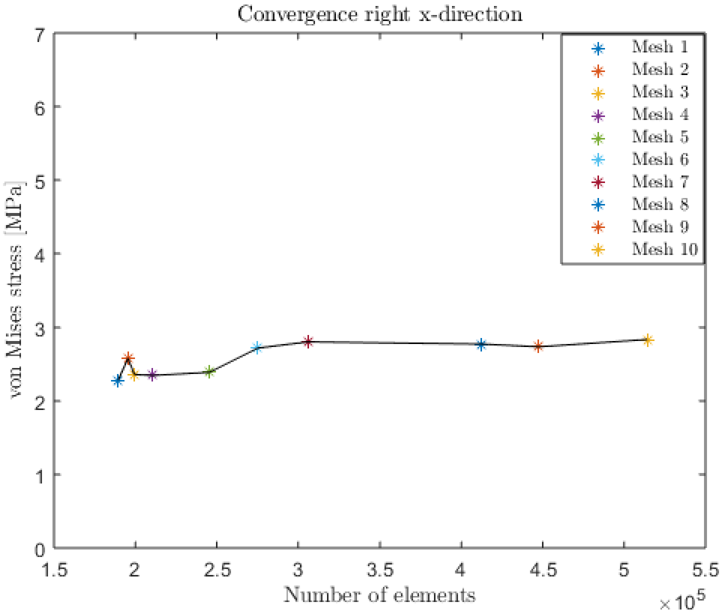

Figure 4.4: Mesh convergence for stress predictions related to external loads applied in the x-direction in the right bushing.

Figure 4.5 shows the convergence results for stresses obtained from pretension only. The stresses from pretension converge for Mesh 6 again, with a deviation for Mesh 10. The deviation is presumably due to local mesh refinements that were not correctly executed. The stress convergences for the external loads in the other directions can be observed in Appendix A. It can be observed in Appendix A that Mesh 10 does not deviate for these cases; this is since other areas have been employed in these convergence studies.

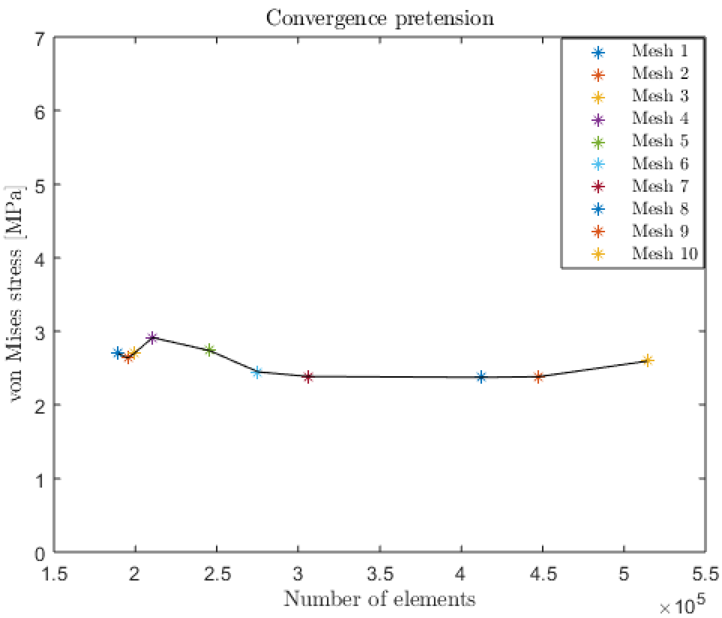

Figure 4.5: Mesh convergence for stresses from pretension.

4.2.2 Static analyses

The results from the linear elastic analysis were analyzed to identify where stress concentrations arose and where fatigue was at most risk to appear. Results from the static analysis can be investigated in Figure 4.6 and Figure 4.8. For stress result plots from the external loads in the other directions, see Appendix B. The absolute maximum principal stresses were used to investigate whether the stresses were compressive or tensile.

It was found that the highest stresses from the unit loads occurred in the radius to the left in Figure 4.6.

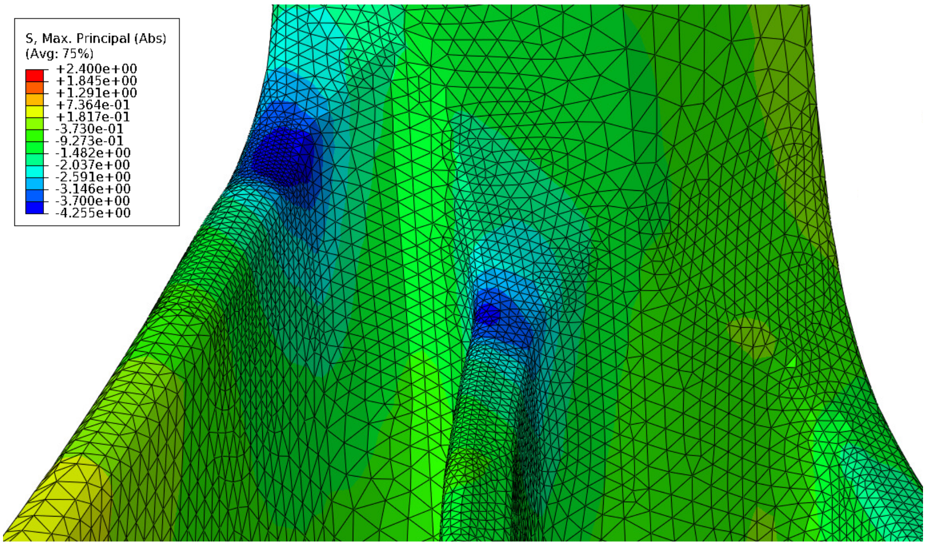

Figure 4.6: Static analysis for loads applied to the right bushing in the x-direction.

The highest stresses that arose from the pretension occurred in the contact area of the bolted joint. The high stresses in the bolted joints could be considered singularities, see Figure 4.7. Those areas were consequently ignored. Instead, the areas close to the bolted joints were investigated.

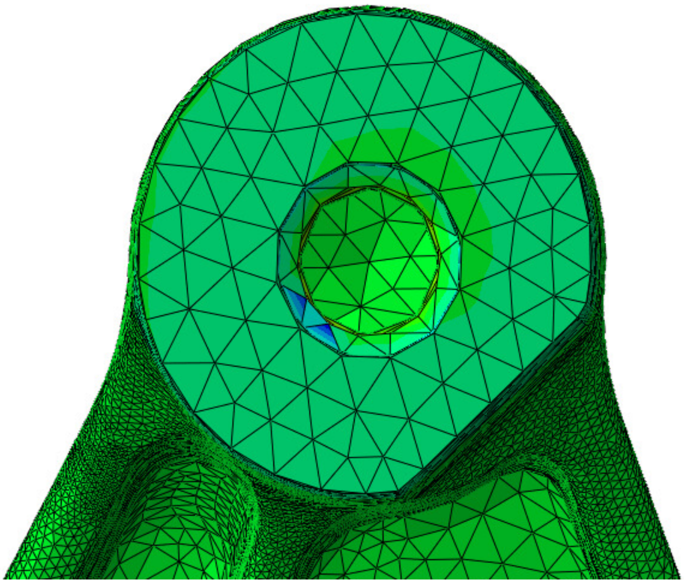

Figure 4.7: Singularities in the contact area of the bolted joint.

Observing the stress results in Figure 4.8, it can be seen that no singularities were present in the investigated areas close to the bolted joints. It can be observed that there were areas where compressive stresses occurred. These were found to be the same areas that featured high stress concentrations in Figure 4.6.

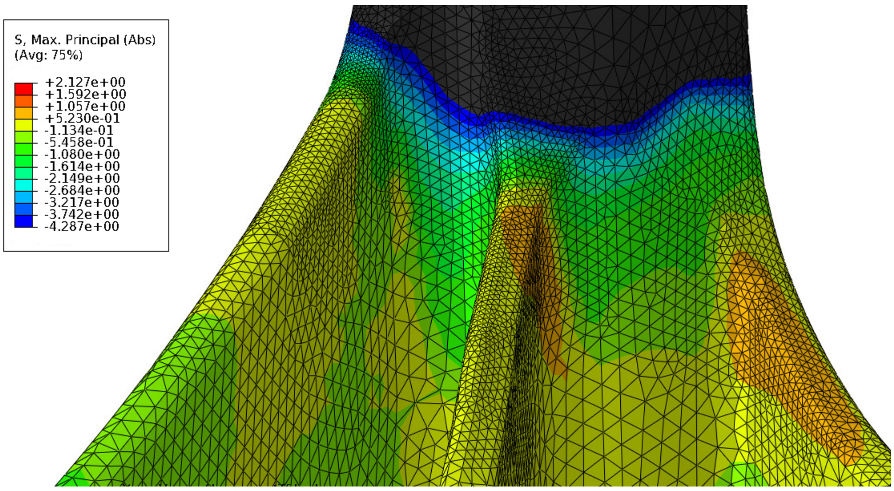

Figure 4.8: Result from static analysis for the pretension.

5
Fatigue analyses

In this study, fatigue analyses were performed in nCode DesignLife 13.1, and a fatigue software called Software1 in this study. The results were post-processed in Meta Version 18.1.4 [35] for fatigue analysis in nCode DesignLife, and in Abaqus/Viewer 2017 for Software1.

5.1 Road Load Data (RLD)

The RLD used for fatigue evaluation of the SB were obtained from simulations in Adams [31] and contained 14 driving events. Each driving event was repeated a certain number of times. The 14 events with the specific repeats replicated a lifetime load sequence for the SB. Three examples of the events are described in Table 5.1.

Table 5.1: Example of driving events.

Event	**Repeats**
Full throttle	10000
Reverse up 8 % slope	800
Cobblestone	4200
...	...

In the RLD, each driving event contained six channels. The channels contained times series for total radial forces in x-, y- and z-direction for both bushings. The RLD was obtained in the same node as the external loads were applied on in the FE-analysis, see Section 4.1.3. An example of RLD is shown in Figure 5.1 and the total radial forces against time for x-, y- and z-directions are shown. The amplitudes vary significantly over time.

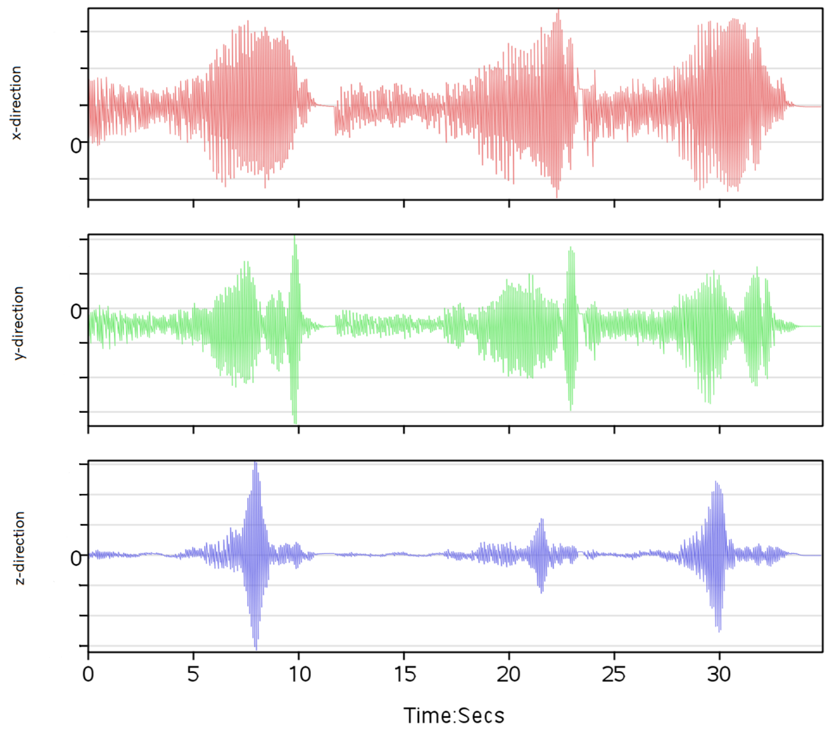

Figure 5.1: Example of bushing RLD for a driving event.

5.2 Method – software abilities

To be able to analyze fatigue, numerical codes for fatigue evaluation had to be selected. The two fatigue software that were compared were nCode DesignLife, and Software1. They were compared by investigating which software that had the most suitable theories for this study. The evaluation was also based on which fatigue software that would be most beneficial for the department Powertrain mounts.

Equivalent settings were used in both fatigue software to make the simulation results comparable. A significant difference was, however, the handling of stresses. In nCode DesignLife the absolute maximum principal stress was employed, while in Software1 the von Mises stress was applied. The strain-based theory was used, see Section 2.5.2. Due to the pretension from the bolted joints, a mean stress correction was applied and the SWT relationship, equation (2.8), was selected. Plastic correction had to be used since an elastic analysis was carried out in Abaqus/Standard. Neuber's rule, equation (2.5), was used for plastic correction.

Each event contained seven load cases, one from the pretension and six from the external loads. The pretension was set to static in all 14 events to prevent it from cycling with the RLD. The six external loads were connected to the associated channel. The procedure of how to handle the loads was different between software; the procedure for nCode DesignLife is explained in Section 5.2.1.

The material data could be obtained from the basic material database or be user-defined. For the fatigue analysis, the material was user-defined to replicate the aluminum alloy EN – 46000 since the alloy did not exist in the basic material database. The material fatigue parameters were estimated using the Bäumel – Seeger method, see Table 2.2.

5.2.1 nCode DesignLife

The fatigue loads were prepared for fatigue analysis by creating a duty cycle. The duty cycle contained 14 driving events from the RLD with time series of total radial forces in x-, y- and z-directions. Each event was repeated a specific number of times.

A flow chart was developed using glyphs in nCode DesignLife, see Figure 5.2. The created flow chart for strain-based fatigue analysis contained three glyphs: FE-Input, E – N analysis, and FE-Display. The results in terms of stresses and strains from the FE-analysis was the input in the FE-input glyph.

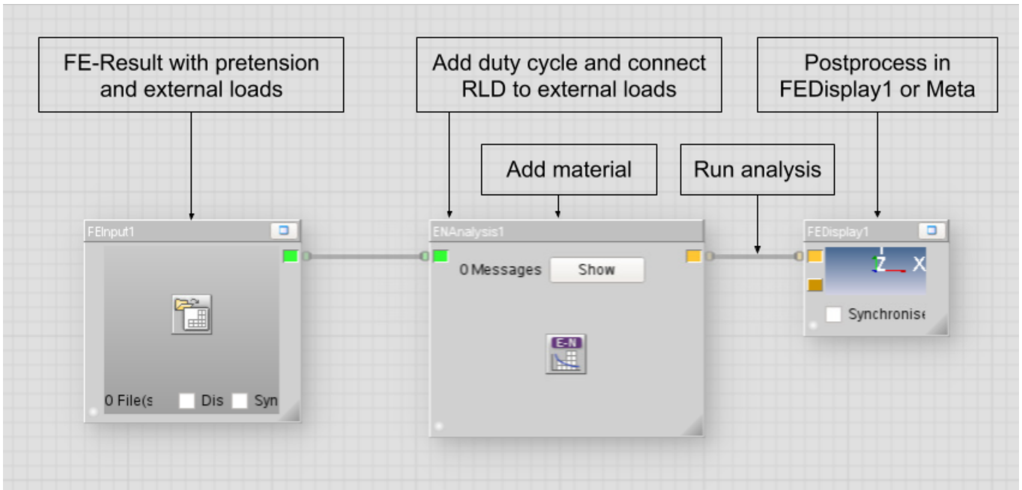

Figure 5.2: The glyph setup for E – N fatigue analysis.

In the second glyph, E – N-analysis, the settings required for the analysis were defined. The loads were applied in this glyph using the created duty cycle. In each driving event of the duty cycle, the external loads, and the associated channel from RLD were connected and the pretension was added as a static load for each event.

A rainflow count (RFC) [24] was performed for all events in nCode DesignLife. The RFC handled each event independently, which was the least time-consuming and least computationally expensive. An example result of the RFC analysis from one channel is shown in Figure 5.3. The histograms show the number of cycles, the range of the loads, and the mean loads. In the figure, the same histogram is shown from different views. The colors represent the number of times the cycles are repeated.

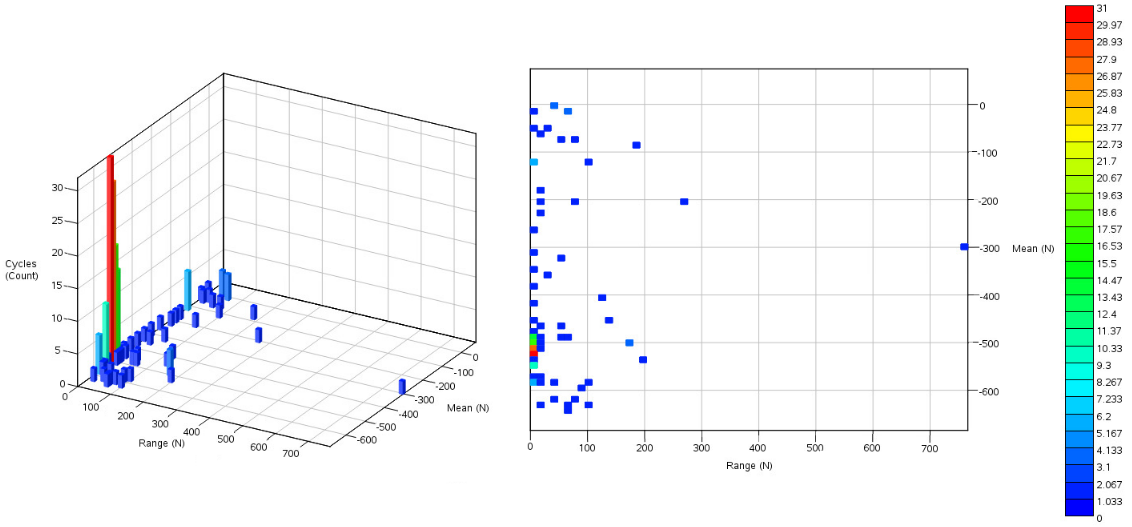

Figure 5.3: Example of histograms from two different views.

Absolute maximum principal stresses and strains were used in nCode DesignLife. The reason for employing absolute maximum principal was due to the limited choice in nCode DesignLife. During the analysis, nCode DesignLife implements Palmgren – Miner's rule to accumulate fatigue damage according to equation (2.2). The results were post-processed in the third glyph, FE-Display and in Meta.

5.3 Result – software abilities

The results from the comparison between nCode DesignLife and Software1 fatigue evaluations featuring unit loads scaled with the RLD are shown in Table 5.2.

Table 5.2: Fatigue results from nCode DesignLife and Software1.

Software	Fatigue life
nCode DesignLife	0.025
Software1	0.012

Since both fatigue software gave similar result, other factors were taken into account when choosing fatigue software for further analyses.The difference in fatigue life was due to von Mises stress being employed in Software1 and absolute maximum principal stress in nCode DesignLife. The option of selecting absolute maximum principal was not available in Software1 and was one reason for choosing nCode DesignLife instead. Other reasons for selecting nCode DesignLife was existing know-how within the company and that the software was more user-friendly. Many events and load cases had to be handled, and that procedure was more straightforward in nCode DesignLife. The process of creating a lifetime sequence was straightforward in nCode DesignLife due to the possibility of generating a duty cycle. The created duty cycle was then accessible when changing FE-model or changing settings.

5.4 Fatigue analysis

The following fatigue analyses were performed in nCode DesignLife. All fatigue analyses, except Section 5.5 and Section 5.9.1, were performed with surface roughness "as cast", see Table 2.3. Mesh 9 was employed in all fatigue analyses (with the exception of the mesh convergence study).

5.4.1 Summary of methodology

The methodology that was used in the fatigue analyses was the same as for when comparing the fatigue software. The method is explained in detail in Section 5.2.1 and Figure 5.2 describes the procedure implemented in nCode DesignLife. The main settings are summarized in Table 5.3.

Table 5.3: Main settings for nCode DesignLife.

Parameter	Settings
Approach	Strain-based
Strains	Absolute maximum principal
Mean stress correction	SWT
Elastic-plastic correction	Neuber's rule

5.4.2 Method – subframe bracket

Bolts, bushings, and subframe were excluded from the fatigue analyses, although they were included in the FE-analysis to obtain the load transfer through the bushings. The subframe was needed to retain the stiffness of the SB, and the bolts were required to obtain the pretension. The parts were excluded from the fatigue analyses since merely the SB had to be analyzed for fatigue.

Four modifications of the fatigue analyses were carried out. These are summarized in Table 5.4. The fatigue analyses were carried out with unit loads and non-unit loads scaled with the RLD. The SB was also evaluated without and with the pretension.

Table 5.4: Analyzed load cases.

Load cases
Unit loads scaled with RLD with pretension
Unit loads scaled with RLD
Non-unit loads scaled with RLD with pretension
Non-unit loads scaled with RLD

5.4.3 Result – subframe bracket

In the fatigue analyses with unit loads scaled with RLD and pretension, the shortest life appeared in the bolted joint and was 0.0250 lives, see Table 5.5. As discussed, the reason for fatigue predicted in the bolted joint was due to the singularities, and the result was therefore considered as inaccurate. The singularities did not appear in the areas with stress concentrations from static loading, see Figure 4.7 for position of singularities.

Table 5.5: Fatigue results of the load cases.

Load cases	Fatigue life	Placement
Unit loads scaled with RLD with pretension	0.0250	Bolted joints
Unit loads scaled with RLD	∞	-
Non-unit loads scaled with RLD with pretension	0.0020	Critical areas
Non-unit loads scaled with RLD	0.0019	Critical areas

It was observed in Section 4.2.2 that stress concentrations arose in the radii; however, the stresses were also low in those regions. Low stress concentrations in combination with unit loads that were scaled with the RLD which contained low loads resulted in infinite lives.

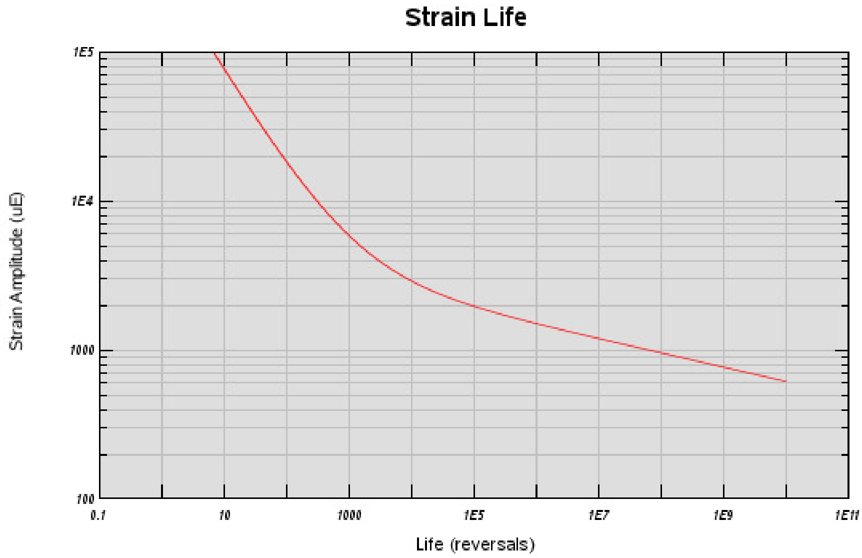

Figure 5.4: E−N curve for approximated EN−46000.

Non-unit loads scaled with RLD were employed to investigate the areas where fatigue would appear under operational conditions. Regardless if the pretension was present or not, fatigue occurred in the regions with stress concentrations identified in the static analysis. Loading with and without pretension resulted in approximately the same fatigue life, see Table 5.5. The reason for obtaining roughly the same result was due to that the stresses from the pretension were low compared to the stresses from the non-unit loads scaled with RLD.

5.4.4 Method – element set of subframe bracket

Based on the results from previous section, an element set was created containing the SB but excluding the contact area of the bolted joints and the contact surfaces, see Figure 5.5a and Figure 5.5b. It was crucial to be able to include the stresses from the pretension in the fatigue analyses, without having to take the contact area of the bolted joints (where the singularity had occurred) into consideration. Figure 5.5b shows the established element set where it can be observed that the contact areas of the bolted joints have been completely removed. In the fatigue analysis underlying Figure 5.5b, unit loads scaled with RLD and pretension were applied.

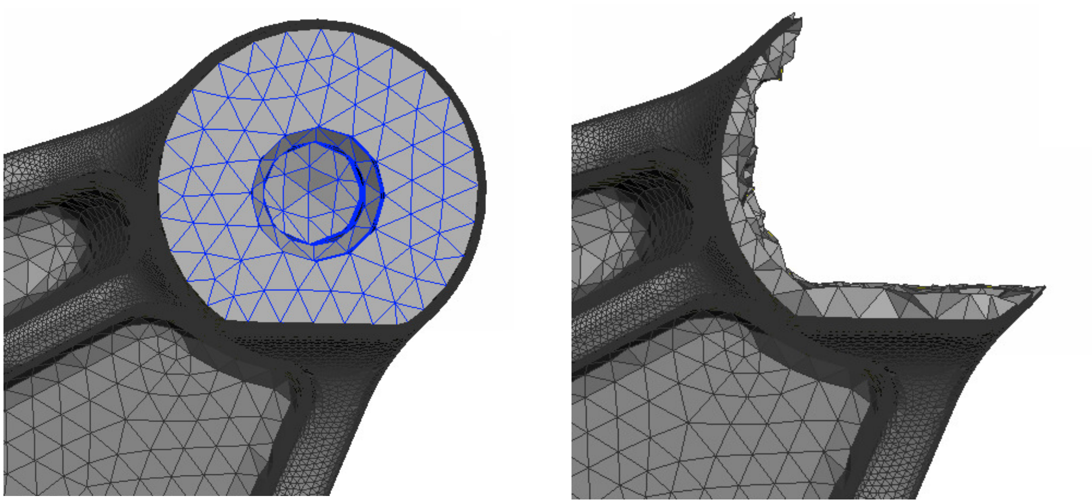

(a) Element set disabled. **(b)** Element set enabled.

Figure 5.5: Part of the bracket with a) element set disabled and b) element set enabled.

5.4.5 Result – element set of subframe bracket

Utilizing the element set for fatigue analysis resulted in infinite lives for unit loads scaled with RLD and pretension, see Figure 5.6. The reason that the SB sustained an infinite number of load cycles was since the singularities were removed. As mentioned in Section 5.4.3, the stresses were not high enough to result in any damage. Even though the stresses from the pretension were accounted for, the stresses from pretension were low as well.

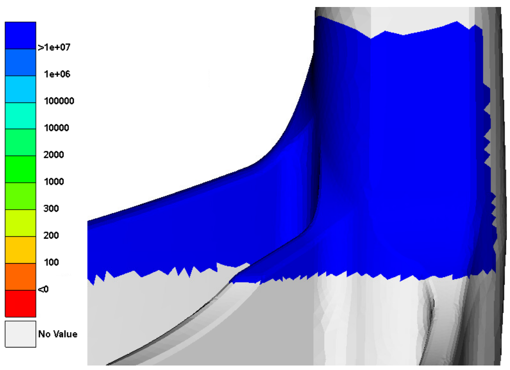

Figure 5.6: Fatigue result of the SB.

5.5 Method – mesh dependency on fatigue predictions

A mesh convergence for fatigue life predictions was carried out with the same meshes as in Table 4.1. The reason for carrying out another mesh convergence study was to investigate the effect of stress and strain magnitudes on fatigue life. If the stresses would not converge, it would give a more significant difference in result for the fatigue analysis since fatigue life decreases exponentially with stress and strain magnitudes.

Non-unit loads scaled with RLD and pretension were used to obtain a result as close to 1 life as possible for Mesh 1. The surface roughness "polished" was employed since it was the default setting in nCode DesignLife, and the effect of surface roughness was not investigated. The element set created in the previous section was implemented to ignore areas with singularities.

5.6 Result – mesh dependency on fatigue predictions

Figure 5.7 shows the fatigue life for the ten meshes. It can be observed that the fatigue life levels out with a finer mesh. The slight differences between the fatigue life for the meshes were sufficiently small that it could be concluded that the fatigue life has converged for Mesh 6. Mesh 10 is a deviation, as mentioned earlier, that is due to local refinements that have not been executed correctly. This affected the stresses and therefore also the fatigue life.

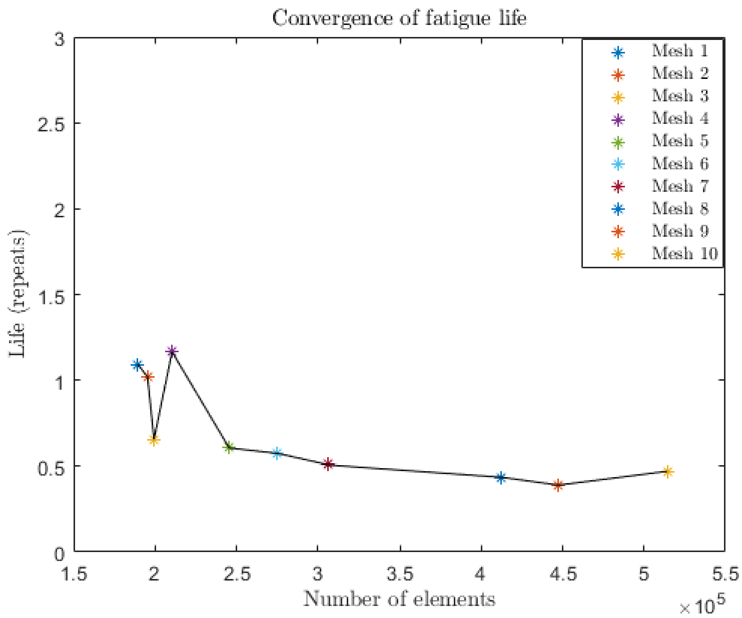

Figure 5.7: Convergence of predicted fatigue life with mesh size.

5.7 Method – lives to failure

In Section 5.4.5, it was established that analyzing fatigue with the unit loads scaled with RLD resulted in infinite lives for the SB. Instead, an investigation of how much larger the loads could be to sustain 4 lives was carried out. 4 lives were chosen as a safety factor due to uncertainties in the material fatigue data. To establish the corresponding load, an iteration was performed. The iteration was performed using Mesh 9 since it provided a sufficiently fine resolution.

5.8 Result – lives to failure

For the SB to sustain 4 lives, the loads could be approximately 2.4 times larger. The fatigue result is shown in Figure 5.8, where it can be seen that two of the three radii are affected by fatigue. The area where fatigue life occurred had the same placement as to where high compressive stresses arose in the static analysis. Compressive stresses do not contribute to fatigue, but in this study, it was the RLD that defined if the stresses became compressive or tensile. Therefore, it was not enough to investigate where the tensile stresses appeared in the static analysis to predict where fatigue would occur. The areas that were affected by stress concentrations had to be investigated, regardless it the stresses were compressive or tensile in static analysis. The cause for fatigue being predicted in areas where the stresses in the static analysis were compressive was due to the dominant negative forces in the RLD. Negative RLD forces would then correspond to tensile stresses.

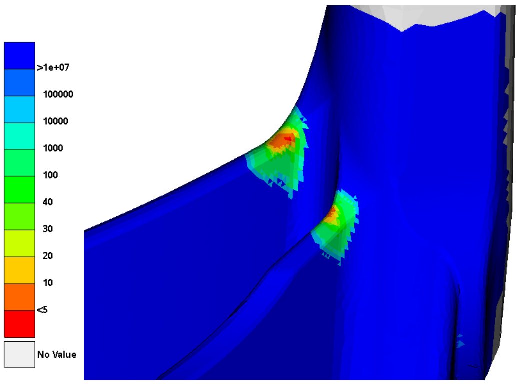

Figure 5.8: Fatigue results for load magnitudes resulting in 4 lives.

5.9 Method – sensitivity analyses

The impact of surface roughness and other parameters that were presumed to have a significant effect on fatigue life were investigated. The investigation was carried out by comparing results of the fatigue analyses when changing the parameters of interest.

5.9.1 Surface roughness

To investigate how much the fatigue life of the SB was affected by surface roughness, different surface finish conditions were utilized in fatigue analyses. The conditions defined by nCode DesignLife (described in Table 2.3) were used. The surface roughness was managed in nCode DesignLife with the average depth of roughness parameter, Rz.

Non-unit loads scaled with RLD and pretension were used for this study to obtain fatigue in the SB. It was assumed that the surface roughness condition "as cast" would give the shortest fatigue life and therefore, "as cast" was used to benchmark how large the load had to be to obtain 1 life. The same loads were applied for all surface roughness conditions. To save computational time the study was performed on Mesh 1, see Table 4.1.

5.9.2 Fatigue material data

Two different analyses were executed. The first analysis investigated the independent influence of the material fatigue parameters for the strain-based approach to fatigue. For the second analysis, three sets of material fatigue parameters were applied in the analyses. Two sets were obtained from approximation methods while the third set was obtained from a supplier.

5.9.2.1 Variation of material fatigue parameters

According to the Bäumel – Seeger method, UTS affects the fatigue strength coefficient, σ_f', which consecutively affects the E – N curve. The effect can be estimated from equation (2.7).

The Bäumel – Seeger method states that the material parameters ϵ_f', b, and c, are constant regardless of aluminum alloy, see Table 2.2. However, studying the material database of nCode DesignLife (not approximated with Bäumel – Seeger), it can be observed that the parameters vary between aluminum alloys. Therefore a study was conducted to analyze how significant the effect was when the parameters vary. All the material fatigue parameters will affect the slope of the E – N curve.

Four graphs were created with equation (2.7), computing strain amplitudes, ϵ_a. Each graph had one varying material fatigue parameter while the rest of the fatigue parameters remained the same. The varying parameters were fatigue strength exponent, fatigue strength coefficient, fatigue ductility exponent, and fatigue ductility coefficient. The material fatigue parameters varied in the range found for aluminum alloys and were compared to the parameters obtained from the Bäumel – Seeger method.

5.9.2.2 Sets of material fatigue parameters

Material parameters established using the Medians method (see Section 2.5.4) and from Parameters1 were compared to the Bäumel – Seeger method. Parameters1 are material fatigue parameters for aluminum alloy EN – 46000 that were received from a supplier and have been manipulated due to confidentiality reasons. When comparing the fatigue life predicted using material parameters from the Medians method, Bäumel – Seeger and from Parameters1, loads of 2.4 times larger than the unit loads were applied. The loads of 2.4 times larger than unit loads scaled with RLD were applied to not obtain infinite life with Bäumel – Seeger method.

Table 2.2 shows the material fatigue parameters for EN – 46000 that were used in the analyses when comparing the Medians method, the Bäumel – Seeger method, and Parameters1. For the Medians method, n′ and K′ were calculated using equation (2.12). The variation in material fatigue parameters in Section 5.9.2.1 does not take the relationship between the material parameters into account, each parameter was evaluated independently. Therefore, the influence of the three material fatigue parameters in Table 5.6 was analyzed. It can be observed that parameter b, c, n′, ϵ'_{f} and σ'_{f} deviates from the approximation method's parameters.

Table 5.6: Material fatigue parameters for EN – 46000.

Parameters	Bäumel – Seeger method	Medians method	Parameters1
σ_u [MPa]	240	240	265
E [MPa]	70000	70000	70000
σ_0 [MPa]	140	140	152
σ'_f [MPa]	401	456	779
ϵ'_f	0.35	0.28	0.0052
b	-0.095	-0.11	-0.12
c	-0.69	-0.66	-0.503
n'	0.11	0.167	0.056
K' [MPa]	387	564	312

5.10 Result – sensitivity analyses

The results obtained from the sensitivity analyses regarding surface roughness and material fatigue parameters are described below.

5.10.1 Surface roughness

The resulting fatigue life for the different surface roughness conditions is shown in Table 5.7. The surface roughness conditions "poor machined" and "as-rolled" were not analyzed since they had the same Rz value as the condition "as cast".

Table 5.7: Results of fatigue life for surface roughness conditions.

Conditions	Rz [μm]	Fatigue life
Polished	0	5.69
Ground	12.5	2.42
Machined	100	1.26
As cast	200	1.03

As expected, fatigue life decreases with an increased surface roughness. Although, Table 5.7 shows that the differences in fatigue life are more substantial for changes in low Rz values compared to changes in higher Rz values, where the difference in fatigue life did not vary significantly.

There might be a difference in surface roughness for HPDC and rheocasting, however, such a difference is not accounted for when selecting the setting "as cast". Still, the difference in fatigue life is small for high surface roughness. Therefore it is assumed that the influence of fatigue life due to variations in surface roughness between the two cast methods is negligible.

5.10.2 Fatigue material data

The result from varying material fatigue parameters one at a time is presented below. Three sets of material fatigue parameters were available.

5.10.2.1 Variation of material fatigue parameters

From the created graphs seen in Figure 5.9 and in Appendix C, it could be interpreted how much the change in a fatigue parameter affects the fatigue life. The graphs indicate that a small change in material fatigue parameter values has a significant effect on predicted fatigue life. The significant effect that the parameters have on fatigue life can be predicted by equation (2.7) and is shown in Figure 5.9 and in Appendix C. Since the material fatigue parameters obtained from the Bäumel – Seeger method are roughly approximated, errors can occur when employing the method. Figure 5.9 and the figures in Appendix C should be interpreted with caution since there is a correlation between all material fatigue parameters.

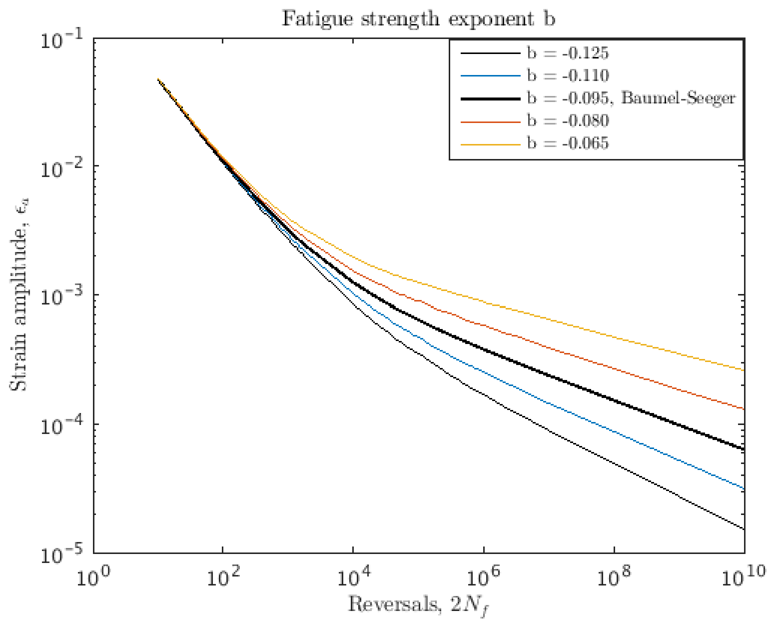

Figure 5.9: Fatigue strength exponent's influence on E−N curve.

There is a difference in material fatigue parameters between the casting methods, HPDC, and rheocasting. Approximating the material parameters does not take the effect of the casting methods on the parameters into account. Due to this, it was not possible to account for the difference in material fatigue properties between the casting methods when analyzing fatigue. If the material fatigue parameters had been retrieved through physical testing, there would be a difference in material fatigue parameters depending on if the casting method was HPDC or rheocasting.

5.10.2.2 Sets of material fatigue parameters

The results from comparing fatigue life with material parameters established using the Medians method, the Bäumel−Seeger method and from Parameters1 are presented in Figure 5.10. The figures show that a more significant area is affected by fatigue for the Parameters1 material data. For all parameter sets the two radii to the left were most affected by fatigue. The right radius was more affected when employing Parameters1 compared to the approximation methods.

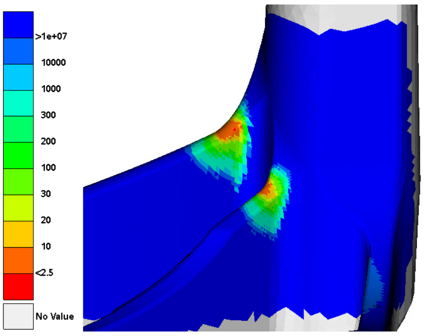

(a) Medians method.

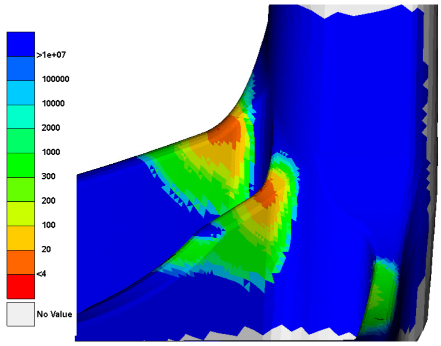

(b) Parameters1.

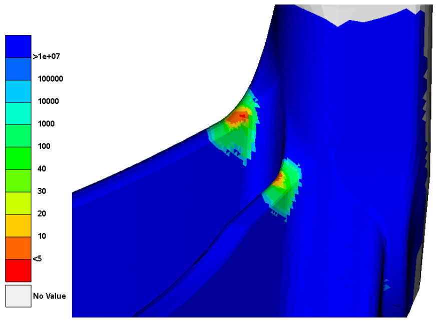

(c) Bäumel – Seeger method.

Figure 5.10: Fatigue life repeats predicted using material parameters obtained using a) Medians method, b) Parameters1 and c) Bäumel – Seeger method.

The fatigue life results for the approximation methods and Parameters1 are shown in Table 5.8. The material fatigue parameters for plotting the E – N curve do not differ significantly between the Medians method and the Bäumel – Seeger method. The reason for obtaining fewer fatigue lives for Medians method, according to Table 5.8 was due to approximation of n′ and K′ according to equation (2.12).

Table 5.8: Fatigue life for sets of material parameters.

Material	Fatigue life
Medians	2.47
Parameters1	3.57
Bäumel – Seeger	4.01

5.11 Method – effect of pretension

An investigation of how the pretension affects the SB fatigue resistance was carried out by analyzing the SB with and without pretension. Mean stress correction (SWT) was utilized regardless of the pretension since the mean stress from the RLD had to be accounted for in fatigue analysis.

The investigation was carried out on the element set. The study was conducted to to understand if the stresses from the pretension would affect the fatigue life, even though the stresses from the pretension were low in the areas around the bolted joints and the contact areas. The loads were 2.4 times larger than unit loads and scaled with the RLD according to Section 5.8. However, the pretension was not multiplied with a factor of 2.4.

5.12 Result – effect of pretension

The predicted fatigue life for the SB with and without pretension is shown in Figure 5.11a and Figure 5.11b. By comparing the two figures, it can be identified that fatigue occurs in the same area regardless if pretension is accounted for in the fatigue analyses.

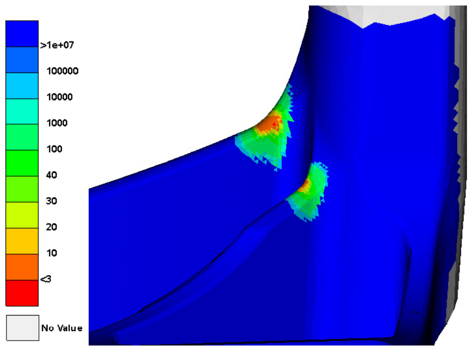

(a) Without pretension.

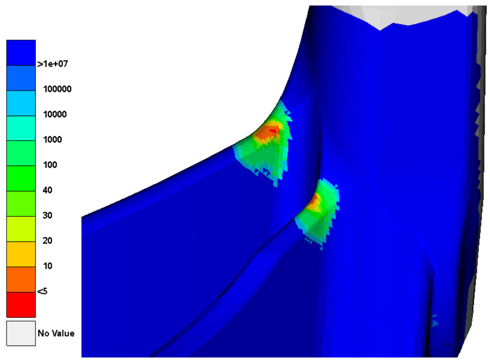

(b) With pretension.

Figure 5.11: Fatigue life predicted a) without pretension and b) with pretension.

The fatigue life when accounting for pretension is longer than when not accounting for pretension, see Table 5.9. Fatigue appeared in the areas where there was compressive stresses from the pretension. Due to these compressive stresses, fatigue life was longer when pretension was applied. The compressive stresses are shown in Figure 4.8.

Table 5.9: Fatigue life with and without pretension.

Load case	Fatigue life
2.4 x unit loads scaled with RLD with pretension	4.01
2.4 x unit loads scaled with RLD without pretension	2.85

5.13 Method – comparison of fatigue approaches

Since no plasticity occurred in the SB during extreme loading conditions, a stress-based fatigue approach was also implemented. For the strain-based fatigue analyses, the utilized settings are described in Section 5.4.1. The strain-based approach and stress-based approach required different material parameters. For the strain-based approach, Parameters1 (see Table 5.6) were employed, and for the stress-based approach, an S – N curve for EN – 46000 was obtained from a supplier. These were obtained from physical testing. Comparing the strain-based approach to stress-based approach would therefore give an understanding of whether the strain-based results gave sufficiently accurate results.

For the two approaches, different mean stress corrections were applied. SWT was used for the strain-based approach, and Goodman for the stress-based approach. SWT is more suitable for aluminum alloys but was not available in nCode DesignLife for the stress-based approach to fatigue. Unit loads scaled with RLD were employed for both strain-based and stress-based approach.

5.14 Result – comparison of fatigue approaches

Different results were obtained from the strain-based approach and the stress-based approach. For the strain-based approach to predict fatigue in the SB, a longer life is obtained compared to a stress-based approach. Comparing Figure 5.12a and Figure 5.12b, it can be observed that a more substantial area is predicted to be affected by the stress-based approach. The area affected in the strain-based approach is very concentrated. However, the shortest predicted fatigue life appears in the same area.

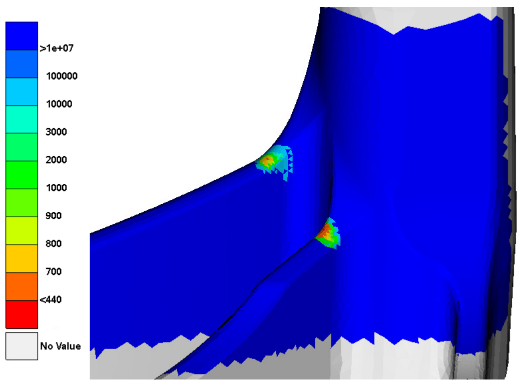

(a) Strain-based approach.

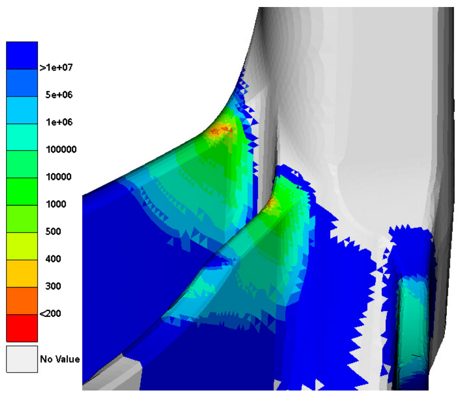

(b) Stress-based approach.

Figure 5.12: Fatigue life predicted using a) strain-based approach and b) stress-based approach.

Even though the difference was significant between the strain- and stress-based fatigue predictions, both approaches predicted that the component met the requirements for fatigue resistance. Since the strain-based approach to fatigue can account for plasticity (if needed for future analysis) and gave a sufficiently accurate result, it was considered to be the most appropriate method to use.

5.15 Method – validation

The method with the strain-based approach summarized in Section 5.4.1 had to be validated. The SB was still in the concept design phase, and no physical component was available. Therefore, it was not feasible to verify the results with physical testing. Instead, an older concept prototype of a bracket was used for validation. The bracket contained bolted joints. Accordingly the pretension had to be accounted for as in earlier analyses. It was known that the bracket used for validation had been tested and a crack had been found after disassembling the component after the tests at the proving ground.

Static analysis with extreme driving events had been investigated for the bracket. From the investigation, it could be observed that a specific area was not meeting the stress level requirements. The areas with the highest stresses were identified, and an expected area for fatigue initiation was identified.

The same fatigue analysis procedure, which was created for the SB was implemented on the bracket used for method validation. The aluminum alloy EN − 46000 was used with parameters from Parameters1. External loads were applied on the bracket in the same nodes where the RLD were obtained from simulations. The RLD contained 18 events, and a duty cycle was created with a specific number of repeats for each event.

5.16 Result – validation

The areas that are highly affected by stresses are shown in Figure 5.13. No singularities appeared in the bolted joints and therefore no element set was created. The figure displays the absolute maximum principal stress, and higher compressive stresses appear in the bracket. From testing at the proving ground, the bracket failed where the compressive stresses are high in Figure 5.13. It is not established if the failure was due to plastic collapse, fatigue, or a combination of both. Presumably due to a combination of both. The stresses in Figure 5.13 have been normalized.

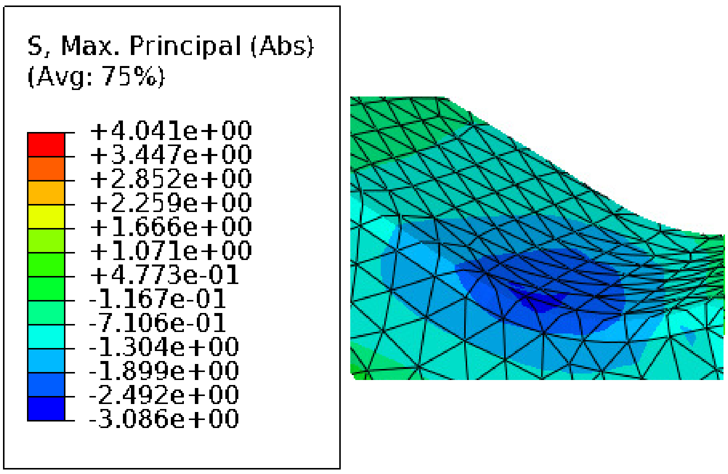

Figure 5.13: Appearance of compressive stresses in the bracket.

The fatigue analysis of the bracket showed that the bracket would fail due to fatigue after 30 lives (see Figure 5.14) with unit loads scaled with the RLD and pretension accounted for in the fatigue analysis. The fatigue arose in the same areas as where the high compressive stresses occurred according to the static analysis and where the bracket failed at the proving ground. If lower fatigue life is obtained and then a few extreme static loads appear on the component it could result in earlier failure than the fatigue analysis indicated.

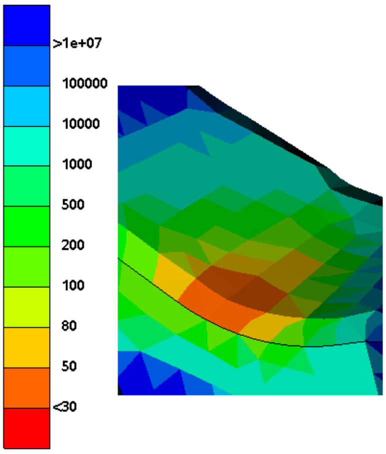

Figure 5.14: Predicted fatigue life.

5.17 Guidelines

During this study, a document with instructions on how to perform a fatigue analysis in nCode DesignLife according to Section 5.4.1, was created. The guidelines provide step-by-step information about all the necessary steps for the FE-analysis and the fatigue analysis. The major parts of the guideline describe how to:

- obtain stress results using perturbation steps for the external loads in the FE-analysis.
- the pretension is fixed in the FE-analysis.
- create a duty cycle, and how to save it for usage in future fatigue analysis.
- connect the external loads to the RLD.
- account for the mean stress that arises from the pretension.
- select the settings for a strain-based approach to fatigue.
- implement the material fatigue parameters.

The guidelines were developed to ease the work for the Powertrain mounts department. To further simplify the procedure of the fatigue analysis, a flowchart was created in nCode DesignLife with the settings predefined. Therefore it is only necessary to insert the results from the FE-analysis and generate a duty cycle to connect the RLD with the applied external loads.

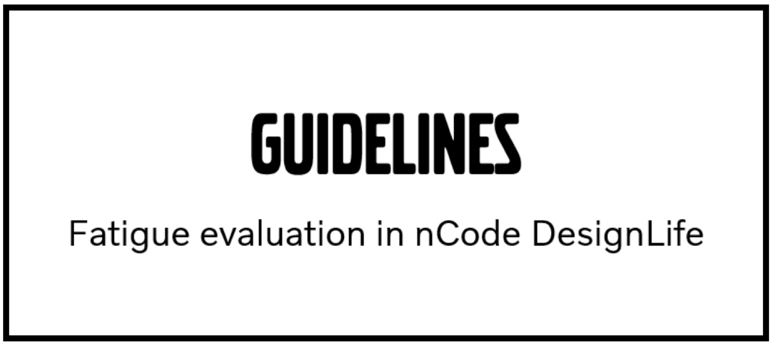

Figure 5.15: Cover of the guideline.

6

Discussion and conclusion

6.1 Discussion

Material fatigue parameters affect the predicted fatigue life significantly and are therefore crucial for fatigue analysis. However, obtaining material fatigue parameters through physical testing is expensive and time-consuming. There is a lack of material fatigue parameters for aluminum alloys in the industry, and therefore, the material fatigue parameters have to be approximated. During this study, two approximation methods for $EN-46000$ were employed for fatigue analysis and the predictions using these material fatigue parameters were compared to predictions featuring material parameters from a data base. Studying Figure 5.9 and Appendix C, it can be established that changes in the material fatigue parameters have a direct effect on predicted fatigue life. Based on these results, it is clear that there are uncertainties in the fatigue analysis. If the predicted fatigue life is close to requirements, the results should be analyzed with caution. For the final evaluation of fatigue, it is then necessary to use more accurate material parameters. The fatigue results will however indicate where fatigue will occur, regardless of uncertainties in the material fatigue parameters.

Analyzing results in bolted joints is complicated due to singularities that can appear. Singularities should not be ignored if they appear in areas that will be analyzed for fatigue. However, if they can be ignored, one option is to create an element set that excludes the contact area of the bolted joints. Employing an element set will ease the post-processing fatigue analysis. However, it is necessary that the bolted joints and contact areas are modeled accurately and not neglected. Not modeling bolted joints will lead to ignoring mean stress from pretension; this will not give accurate predictions since mean stress affects fatigue.

In the SB, the mean stress from the pretension was mostly compressive, and therefore the predicted fatigue life was longer when pretension was considered. The difference in fatigue life with and without pretension was small but increased exponentially when applying lower external loads.

Accounting for pretension, mean stress correction, surface roughness, and approximated material parameters will contribute to the fatigue analysis becoming more accurate. Since it is difficult to know precisely how fatigue software accounts for the fore mentioned parameters, combining the mentioned factors may contribute to a conservative prediction.

There are several benefits with utilizing rheocasting instead of HPDC. One is the reduced cost of not needing pre-cast ingots. Another advantage is the fatigue quality of rheocasting. Neither the fatigue software nor the approximation methods to obtain material account for the corresponding differences in material quality. Therefore it will be challenging to evaluate whether or not the component will have a longer fatigue life when changing the casting method. If the material data had been retrieved through physical testing, a difference in fatigue life would be obtained, since the obtained material parameters would differ between the two cast methods. There is also a variation in surface roughness depending on what cast method that is employed, even though both HPDC and rheocasting have high surface roughness values. In this study, the sensitivity of surface roughness and material fatigue parameters was analyzed. It was stated that fatigue life is moderately affected by high surface roughness values (when comparing Rz 100 μm to 200 μm), while small changes in the material fatigue exponents have a significant effect on fatigue life.

It is generally not necessary to execute a fatigue analysis for each round of development due to the uncertainties in the material parameters. There is a risk of having fatigue failure when optimizing the components with respect to fatigue when there are errors in the material fatigue parameters. Therefore it is more beneficial to perform a fatigue analysis at the beginning of the design process to obtain an indication of what areas will be affected by fatigue.

6.2 Conclusions

The conclusions from the study are:

- One option for ignoring the singularities in the contact area of the bolted joints is to create an element set that excludes the contact areas. The areas with singularities will then not be analyzed in the fatigue analysis.

- Results from fatigue analyses can be heavily influenced by the employed mesh size. It is of importance to refine the critical areas to obtain accurate results.

- The SB met the fatigue requirements regardless of employed material fatigue parameters for EN$-$46000, with the applied loads described in this study.

- Damage is predicted to occur at stress concentrations in the SB with the load cases specified in this study.

- From the validation of the method, the developed fatigue analysis method was found to give reasonable result.

- Due to uncertainties in the material fatigue parameters fatigue analysis in the early design stage should only be used to investigate critical areas and not for optimization.

- The material fatigue parameters have a significant effect on predicted fatigue life; therefore, approximated material parameters should not be used for the final fatigue assessment.

7

Future work

Further investigations are required regarding how the material is effected by the casting method. Rheocasting should increase the quality of the component due to fewer defects. To quantify this effect, an investigation of how the casting method affects fatigue life would be suitable.

A more profound investigation of how to obtain material fatigue parameters is recommended to be executed. The most accurate procedure would be to procure material fatigue parameters through testing.

The bushing contained rubber bushings that were not modeled in this study, although the RLD for the rubber in the bushings were available. Employing the RLD for rubber might have an effect on the fatigue life. Using the RLD for the rubber requires that the rubbers are modeled in the FE-model and that loads are applied to the rubber. Modeling the bushings with rubber and analyzing fatigue in the bracket is another option and might lead to a different result.

Bibliography

[1] M. Gillenäng, "PT school Powertrain mounts system", Unpublished.

[2] H. Klars, "Powertrain mounts system school", Unpublished.

[3] Ståhlberg, W. (2018) Fatigue Life Prediction of Natural Rubber in Engine Mounts. Göteborg : Chalmers University of Technology (Master's thesis - Department of Mechanics and Maritime Sciences, nr: 2018:76).

[4] C. B. Lagrone,"Aluminum (Al)", *Salem Press Encyclopedia of Science*, 2018. Available at: `search.ebscohost.com/login.aspx?direct=true&db=ers&AN=89474551&site=eds-live&scope=site`, accessed on: 2019-02-08.

[5] K. Andersson, J. Weritz, J. Gilbert.Kaufman, "ASM Handbook, Volume 2A - Aluminum Science and Technology" in *ASM Handbook*. [Online]. Available at: `https://app.knovel.com/hotlink/toc/id:kpASMHVAA2/asm-handbook-volume-2a/asm-handbook-volume-2a`, accessed on: 2019-02-11.

[6] J. E. Hatch, *Aluminum: Properties and Physical Metallurgy*, USA: ASM International, 1984. [Online]. Available at: `https://ebookcentral.proquest.com/lib/chalmers/detail.action?docID=3002398`, accessed on: 2019-02-11.

[7] J. G. Kaufman and E. L. Rooy, *Aluminum Alloy Castings - Properties, Processes, and Applications*, USA: AMS International, 2004. [Online]. Available at: `https://app.knovel.com/hotlink/toc/id:kpAACPPAOM/aluminum-alloy-castings/aluminum-alloy-castings` Accessed on: 2019-02-07.

[8] F. M. Mazzolani. *Aluminum alloy structures*. Boston, USA: Pitman publishing limited, 1985.

[9] *Stena aluminum, Alloy specifications*, [Online]. Available at: `https://www.stenaaluminium.com/aluminium-alloys-and-services/alloy-specifications/`

[10] "Pressgjutning" in *Nationalencyklopedin*. [Online]. Available at: `http://www.ne.se/uppslagsverk/encyklopedi/lång/pressgjutning`, accessed on: 2019-02-13.

[11] O. Granath, "Semi-Solid Casting of Aluminum and Magnesium Alloys", Ph.D. dissertation, Department of Materials and Manufacturing, Chalmers University of Technology, Gothenburg, Sweden, 2007.

[12] Y. X. Gao, J. Z. YI, P. D. Lee, T.C. Lindley, "The effect of porosity on the fatigue life of cast aluminum-silicon alloys" *Fatigue & Fracture of Engineering Materials & Structures*. Vol.27. p.559-570. July 2004. doi: 10.1111/j.1460-2695.2004.00780.x, [Online]. Available at: `https://onlinelibrary.wiley.com/doi/full/10.1111/j.1460-2695.2004.00780.x`, accessed on: 2019-02-15.

[13] H. E. Boyer. *Atlas of fatigue curves*, ASM International, USA: Carnes Publication services, 1986.

[14] RheoMetal AB, "Technology, Slurry process". [Online]. Available at: `http://rheometal.com/technology.php`, accessed on: 2019-02-15.

[15] S. P. Midson, A. Jackson. "A Comparison of Thixocasting and Rheocasting" in *World foundry congress, casting the future*, 2006. Available at: `http://www.iftabira.org/pdfs/22%20S.Midson_1360087497.pdf`, accessed on: 2019-02-13.

[16] ASM International Handbook Committee, "Volume 15 - Casting - 92.1 Methods" in *ASM Handbook*. [Online]. ASM International. Available at: `https://app.knovel.com/hotlink/pdf/id:kt008I3Y11/asm-handbook-volume-15/methods`, accessed on: 2019-02-15.

[17] Dassault systems, "Abaqus unified FEA", 2019. [Online]. Available at: `https://www.3ds.com/products-services/simulia/products/abaqus/abaqusstandard/`, accessed on: 2019-06-02.

[18] Abaqus Analysis User's Manual, "General and linear perturbation procedures", 2010. [Online]. Available at: `https://www.sharcnet.ca/Software/Abaqus610/Documentation/docs/v6.10/books/usb/default.htm?startat=pt03ch06s01aus41.html`, accessed on: 2019-04-15.

[19] Abaqus Keywords Reference Guide, "Define a surface-based coupling constraint", 2014. [Online]. Avalilable at: `https://www.sharcnet.ca/Software/Abaqus/6.14.2/v6.14/books/key/default.htm?startat=ch03abk83.html#usb-kws-mcoupling`, accessed on: 2019-05-25.

[20] Abaqus Keywords Reference Guide, "Define surfaces that contact each other", 2010. [Online]. Available at: `https://www.sharcnet.ca/Software/Abaqus610/Documentation/docs/v6.10/books/key/default.htm?startat=ch03abk65.html#usb-kws-hcontactpair`, accessed on: 2019-05-24.

[21] Abaqus Analysis User's Manual, "Defining tied contact in Abaqus/Standard", 2010. [Online]. Available at: `https://www.sharcnet.ca/Software/Abaqus610/Documentation/docs/v6.10/books/usb/default.htm?startat=pt09ch32s03aus139.html`, accessed on: 2019-05-25.

[22] J. Kim, J. Yoon, B. Kang, "Finite element analysis and modeling of structure with bolted joints", *Applied Mathematical modelling*, vol.31, no.5, pp.895-911. July 2006. doi:10.1016/j.apm.2006.03.020, [Online]. Available at: `https://www.sciencedirect.com/science/article/pii/S0307904X0600062X`, accessed on: 2019-03-08.

[23] Tony.A, Joints and Connections in FEA, DE247 Digital Engineering, May. 2014. [Online] Available at: `https://www.digitalengineering247.com/article/joints-connections-fea`, accessed on: 2019-05-24.

[24] N. E. Dowling, *Mechanical Behavior of Materials: Engineering Methods for Deformation, Fracture and Fatigue*. 4th edition, London, United Kingdom: Harlow : Pearson Education, 2013.

[25] R.Basan, M.Franulovic, I.Prebil, R.Kunc, "Strain-life Behavior of Different Groups of Metallic Materials", *Internation Jounral of Fatigue*, vol.33, no.3, March 2011, doi: https://doi.org/10.1016/j.ijfatigue.2010.10.005, [Online]. Available at: `https://www.sciencedirect.com/science/article/pii/S0142112310002409`, accessed on: 2019-05-20.

[26] *DesignLife Theory Guide*, HBM Prenscia, Southfield, Michigan, USA, 2017.

[27] M.A. Meggiolaro, J.T.P Castro, "Statistical evaluation of strain-life fatigue crack initiation predictions", *Internal Journal of Fatigue*, vol.26, no.5, pp. 463-476, May 2004, doi:https://doi.org/10.1016/j.ijfatigue.2003.10.003. [Online]. Available at: `https://www.sciencedirect.com/science/article/pii/S0142112303002469`, accessed on: 2019-05-20.

[28] M. M. Amarala, "Roughness Measurement Methodology according to DIN 4768 Using Optical Coherence Tomography", vol.1, june 2009. [Online]. Available at: `https://www.ipen.br/biblioteca/2009/eventos/14126.pdf`, accessed on: 2019-05-13.

[29] nCode, "DesignLife", 2019. [Online]. Available at: `https://www.ncode.com/`, accessed on: 2019-06-02.

[30] Magna, "FEMFAT software", 2018. [Online]. Available at: `https://femfat.magna.com/welcome/`, accessed on: 2019-06-02.

[31] Msc software, "Adams", 2019. [Online]. Available at: `https://www.mscsoftware.com/product/adams`, accessed on: 2019-06-02.

[32] BETA CAE systems, "ANSA pre processor", 2019. [Online]. Available at: `https://www.beta-cae.com/ansa.htm`, accessed on: 2019-06-02.

[33] Dassault systems, "Abaqus unified FEA", 2019. [Online]. Available at: `https://www.3ds.com/products-services/simulia/products/abaqus/abaquscae/`, accessed on: 2019-06-02.

[34] Mathworks, "MATLAB", 2019. [Online]. Available at: `https://se.mathworks.com/products/matlab.html`, accessed on: 2019-06-02.

[35] BETA CAE systems, "META post processor" 2019. [Online]. Available at: `https://www.beta-cae.com/meta.htm`, accessed on: 2019-06-02.

A

Convergence study

The mesh convergence study with respect to the stresses is shown in Figure A.1 - A.5. The number of elements have increased for each mesh and von Mises stress is compared.

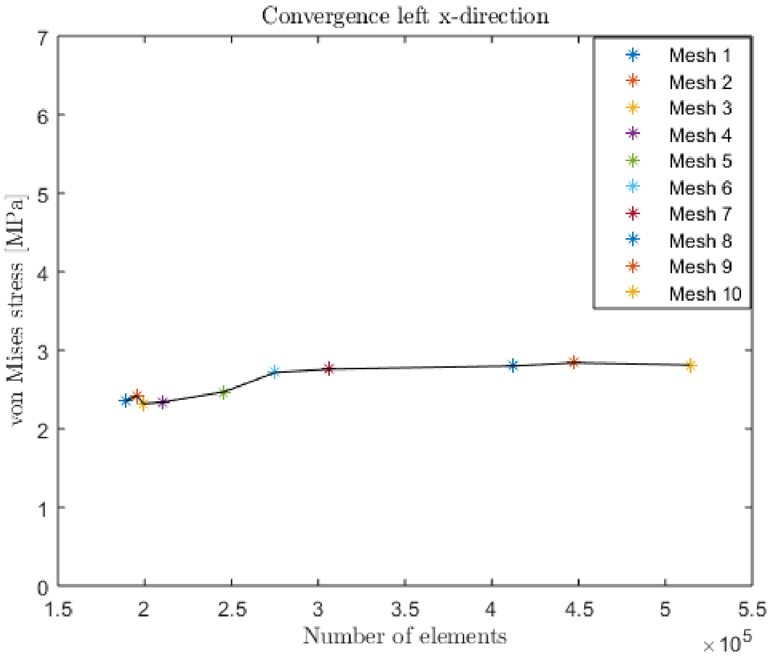

Figure A.1: Mesh convergence for stress predictions related to external loads applied in the x-direction in the left bushing.

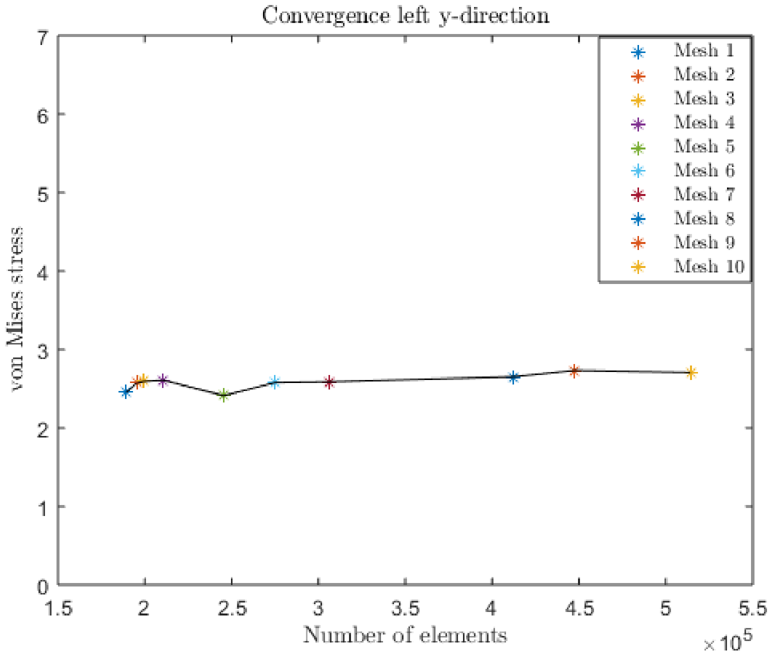

Figure A.2: Mesh convergence for stress predictions related to external loads applied in the y-direction in the left bushing.

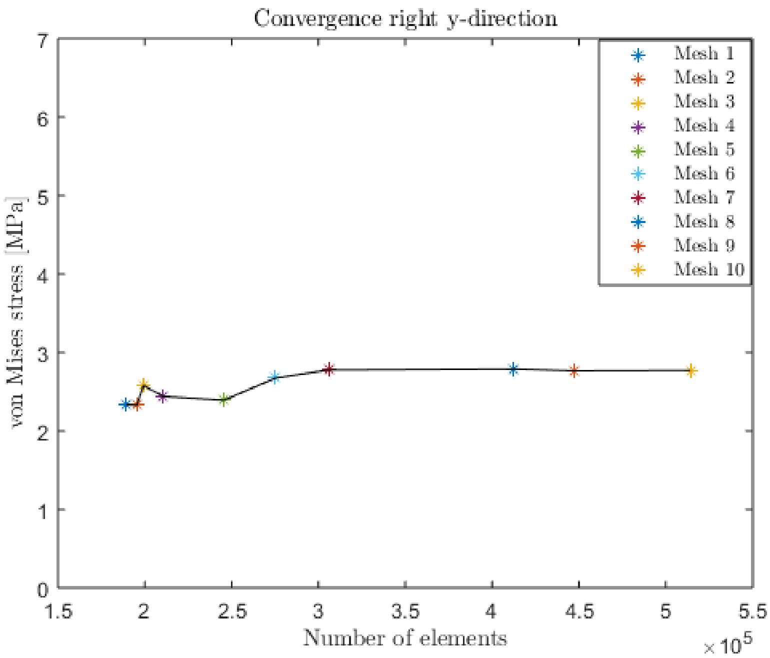

Figure A.3: Mesh convergence for stress predictions related to external loads applied in the y-direction in the right bushing.

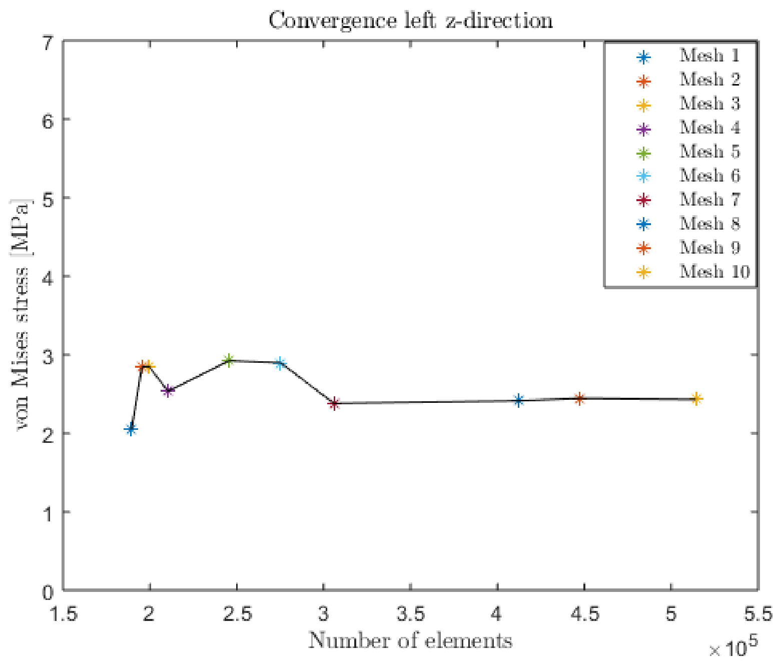

Figure A.4: Mesh convergence for stress predictions related to external loads applied in the z-direction in the left bushing.

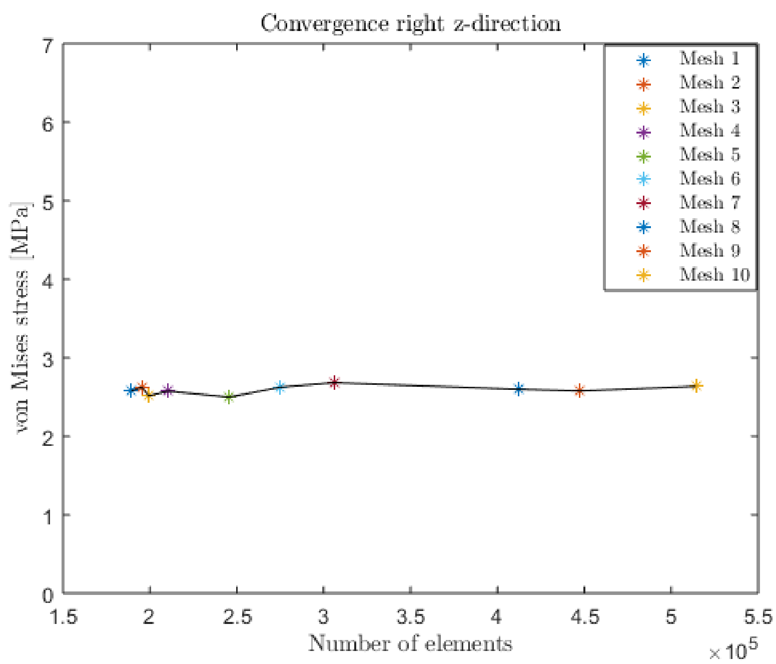

Figure A.5: Mesh convergence for stress predictions related to external loads applied in the z-direction in the right bushing.

B

Static analysis

Figure B.1 - B.5 shows the static analysis when applying external loads in both left and right bushing in all directions. Absolute maximum principal stresses are shown to conveniently see where there are compressive and tensile stresses.

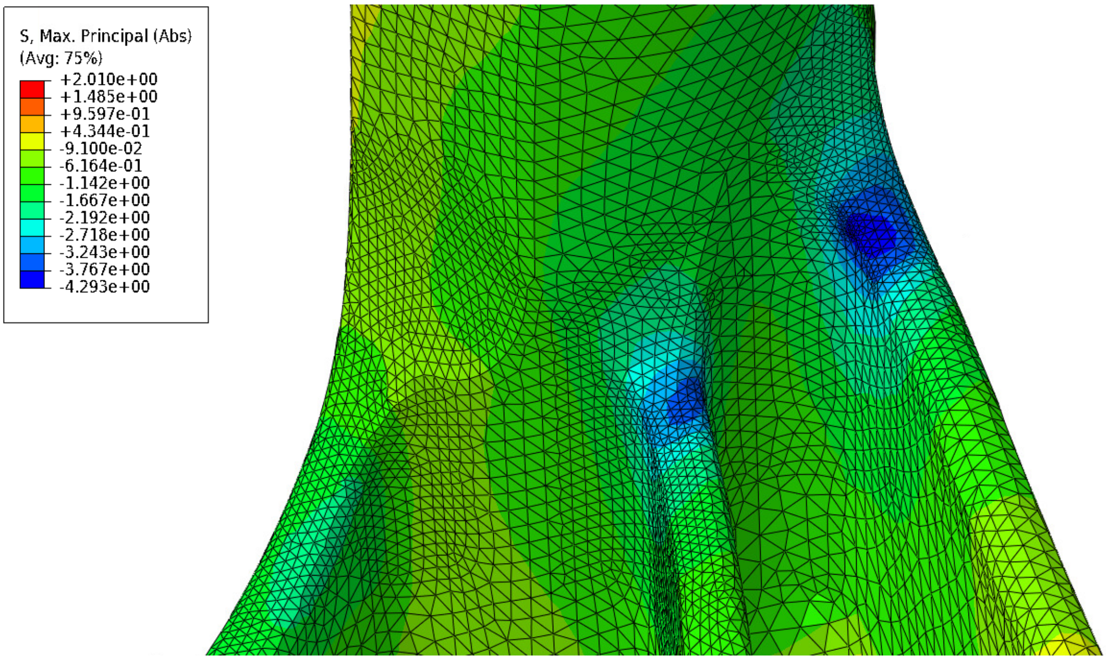

Figure B.1: Static analysis for loads applied to the left bushing in the x-direction

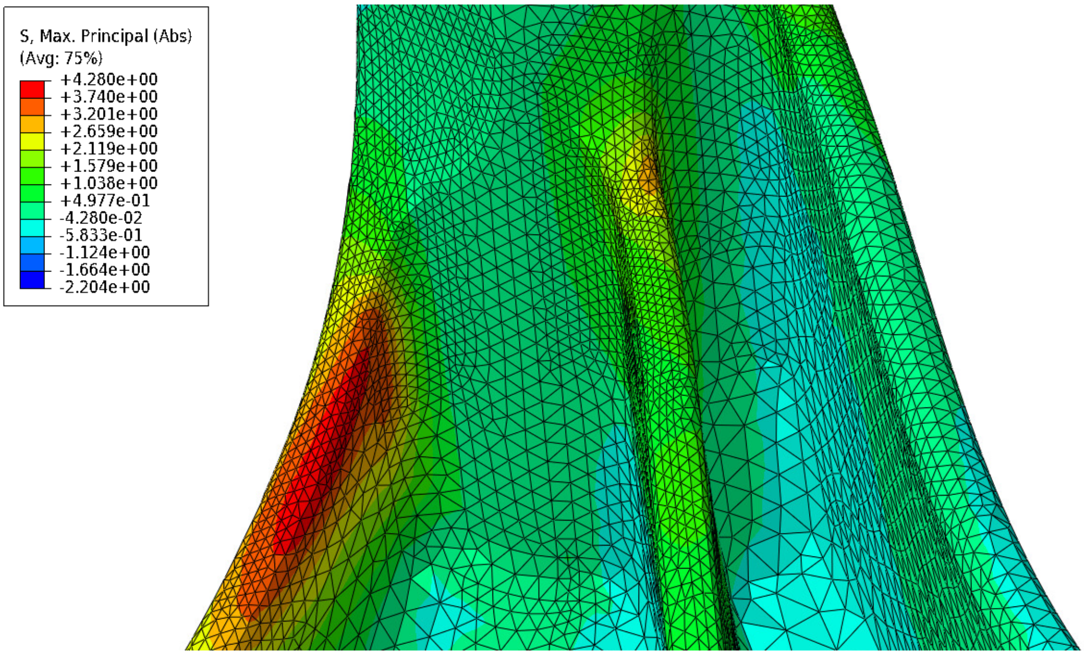

Figure B.2: Static analysis for loads applied to the left bushing in the y-direction.

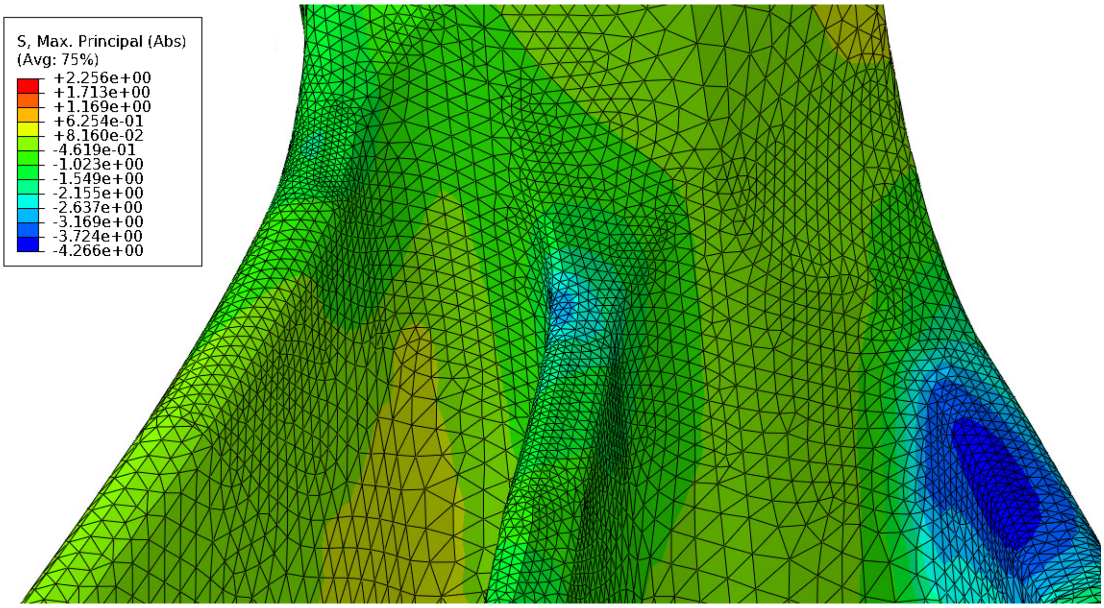

Figure B.3: Static analysis for loads applied to the right bushing in the y-direction.

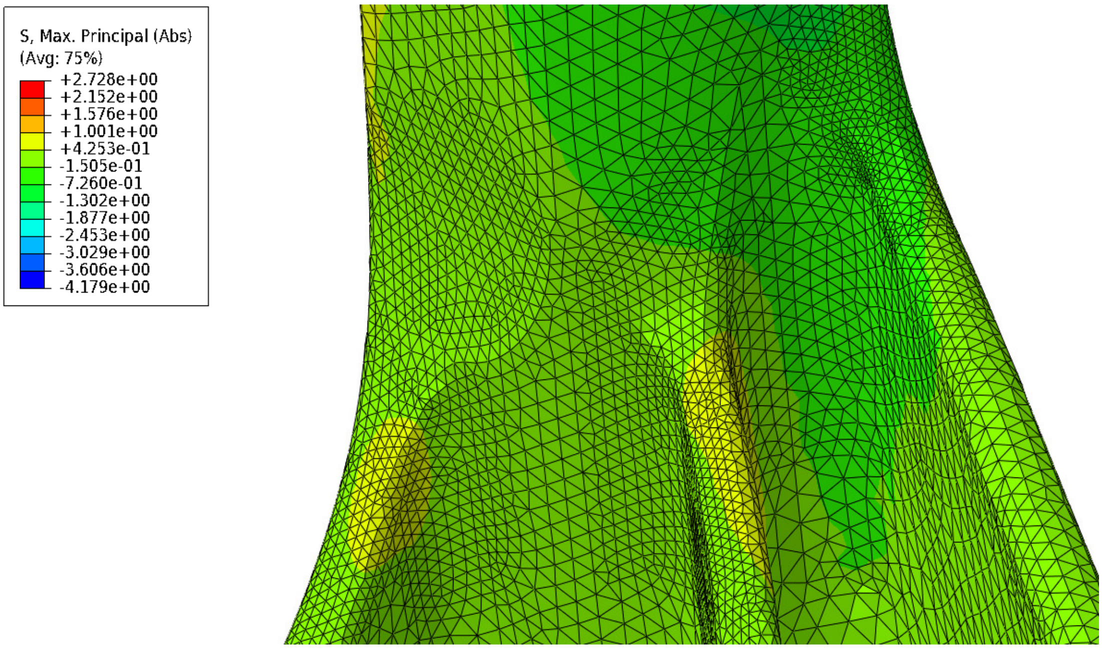

Figure B.4: Static analysis for loads applied to the left bushing in the z-direction.

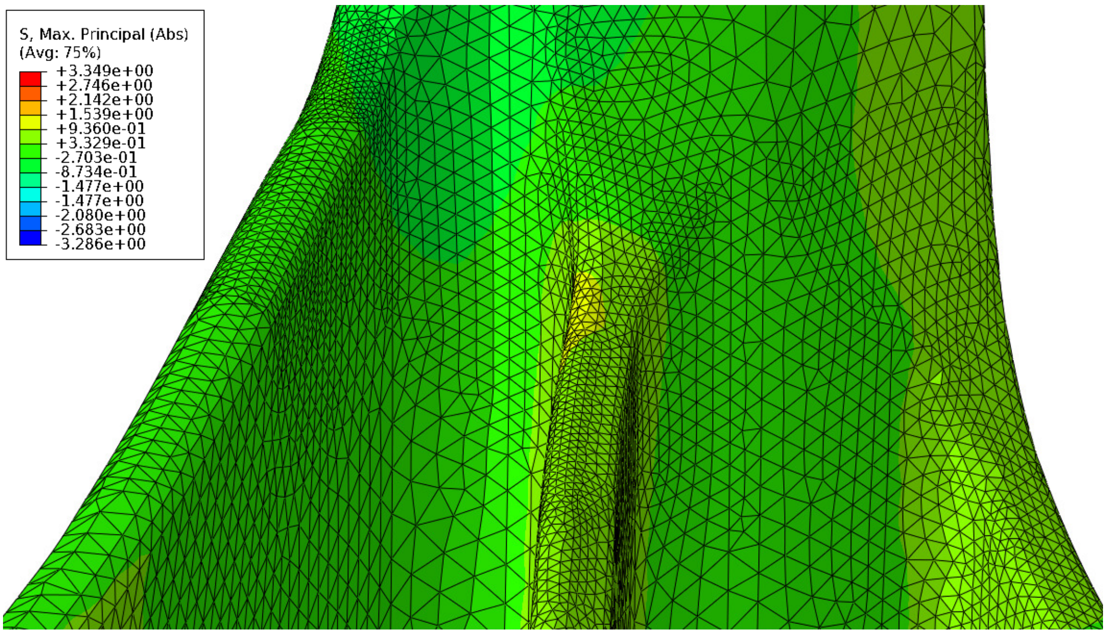

Figure B.5: Static analysis for loads applied to the right bushing in the z-direction.

C
Material parameters

The effect that the material parameters have on fatigue life can be studied in Figure C.1 - C.3. Each figure shows five E−N curves with a variation in the material parameter for each curve.

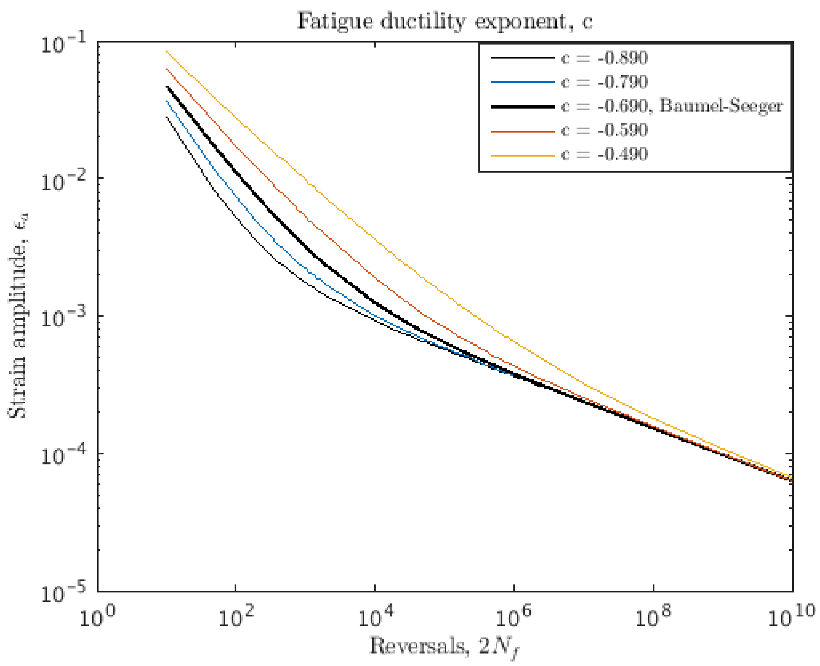

Figure C.1: Fatigue ductility exponent's influence on E−N curve.

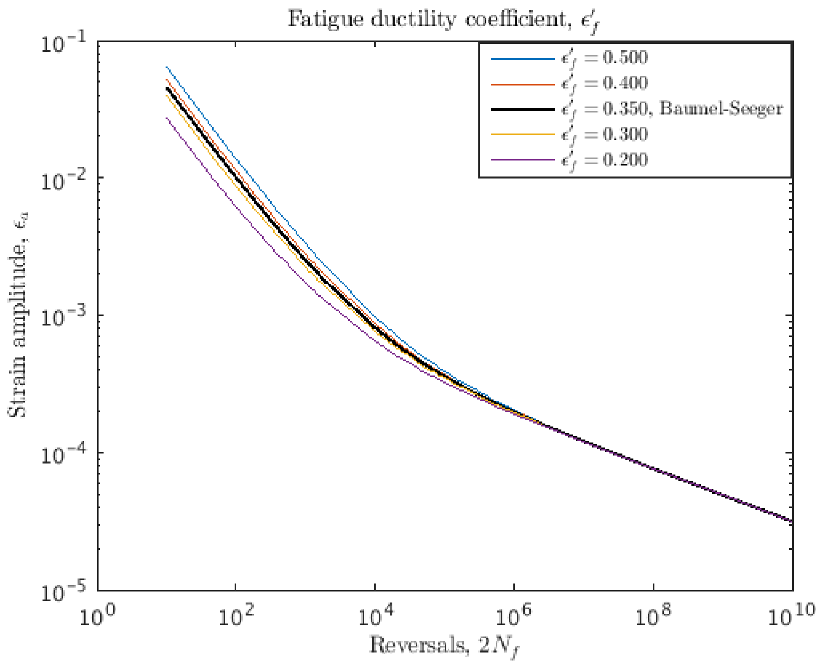

Figure C.2: Fatigue ductility coefficient's influence on E−N curve.

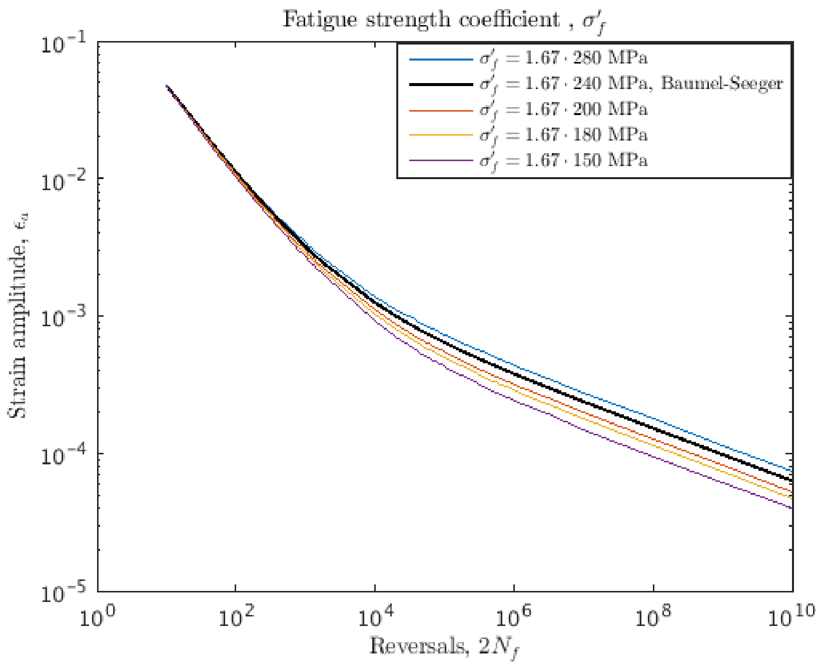

Figure C.3: Fatigue strength coefficient's influence on E−N curve.